04/12/2024 09:34

(Article begins on next page)

Large-scale response of the Eastern Mediterranean thermohaline circulation to African monsoon intensification during sapropel S1 formation

Tesi T. [1, *], Asioli A. [2], Minisini D. [3], Maselli V. [4], Valle G. Dalla [1], Gamberi F. [1], Langone L. [1], Cattaneo Antonio [5], Montagna P. [1], Trincardi F. [1]

[1] CNR, CNR ISMAR, Ist Sci Marine, Via Gobetti 101, I-40129 Bologna, Italy.
[2] CNR, IGG, Via G Gradenigo 6, I-35131 Padua, Italy.
[3] Shell Int Explorat & Prod Inc, 3333 Highway 6 South, Houston, TX 77082 USA.
[4] Univ Aberdeen, Dept Geol & Petr Geol, Kings Coll, St Marys Bldg, Aberdeen AB24 3UF, Scotland.
[5] IFREMER, Geosci Marines EDROME, Ctr Brest, BP70, F-29280 Plouzane, France.

* Corresponding author : T. Tesi, email address : tommaso.tesi@bo.ismar.cnr.it

Abstract :

The formation of Eastern Mediterranean sapropels has periodically occurred during intensification of northern hemisphere monsoon precipitation over North Africa. However, the large-scale response of the Eastern Mediterranean thermohaline circulation during these monsoon-fuelled freshening episodes is poorly constrained. Here, we investigate the formation of the youngest sapropel (S1) along an across-slope transect in the Adriatic Sea. Foraminifera-based oxygen index, redox-sensitive elements and biogeochemical parameters reveal – for the first time – that the Adriatic S1 was synchronous with the deposition of south-eastern Mediterranean S1 beds. Proxies of paleo thermohaline currents indicate that the bottom-hugging North Adriatic Dense Water (NAdDW) suddenly decreased at the sapropel onset simultaneously with the maximum freshening of the Levantine Sea during the African Humid Period. We conclude that the lack of the "salty" Levantine Intermediate Water hampered the preconditioning of the northern Adriatic waters necessary for the NAdDW formation prior to the winter cooling. Consequently, a weak NAdDW limited in turn the Eastern Mediterranean Deep Water (EMDWAdriatic) formation with important consequences for the ventilation of the Ionian basin as well. Our results highlight the importance of the Adriatic for the deep water ventilation and the interdependence among the major eastern Mediterranean water masses whose destabilization exerted first-order control on S1 deposition.

Highlights

► The Adriatic S1 is coeval with the Eastern Mediterranean S1 deposits. ► The Adriatic S1 onset is synchronous with the shutdown of the NAdDW. ► African monsoons weakened the LIW which in turn hampered the NAdDW formation.

Keywords : Sapropel S1, Mediterranean sea, African monsoons, Anoxia, Thermohaline circulation

49

50

51

52

1. Introduction

Periodic perturbations of marine ecology and geochemistry have occurred in the eastern Mediterranean Sea (EMS) since the late Miocene (Nijenhuis et al., 1996). Signs of these changes are preserved in the sediment record as organic carbon-rich deposits commonly known as sapropels. In this study we focus on the most recent sapropel (S1) which formed during the last post-glacial eustatic rise (ca. 10-6 cal kyr BP (De Lange et al., 2008; Hennekam et al., 2014; Schmiedl et al., 2010). It is now largely accepted (Rohling et al., 2015) that favourable conditions for S1 formation were associated with anoxic bottom waters that developed during periods of insolation maxima (Hilgen, 1991; Rossignol-Strick, 1985; Rossignol-Strick et al., 1982). The resulting effect of these orbital variations was the northward migration of the African monsoons resulting in higher precipitation over the Nile river watershed which in turn enhanced the freshwater supply to the EMS southeastern Mediterranean Sea (Hennekam et al., 2014; Weldeab et al., 2014). In addition, the mid-Holocene increase of river runoff from northern borderlands and the post-glacial inflow of less saline Atlantic waters have further contributed to maintaining reduced surface water salinities and high nutrient concentrations in the euphotic zone (Grimm et al., 2015; Kotthoff et al., 2008; Spötl et al., 2010; Toucanne et al., 2015). To date, whether and to what degree either water stratification or enhanced primary productivity has resulted in anoxic bottom waters is still a matter of debate despite several decades of extensive study (Calvert et al., 1992; De Lange et al., 2008; Grimm et al., 2015; Sachs and Repeta, 1999).

A survey of the current literature dealing with S1 reveals that most of the focus has been placed on south-eastern Mediterranean sediments while the Adriatic Sea – that today plays a first-order control on Eastern Mediterranean ventilation (Klein et al., 2000) – has received markedly less interest. In particular,

3

74   it has been suggested (Rohling et al., 1997; Rohling et al., 2015) that the onset of critical oxygen

75   conditions in the Adriatic (ca. 8.8 cal. ky BP) lagged behind the fairly synchronous anoxia which

76   developed over the rest of the EMS (ca. 10 cal. ky BP) (De Lange et al., 2008; Schmiedl et al., 2010). This

77   implies that the ventilation regime under which the Adriatic sapropel formed must have been necessarily

78   different compared to the south-eastern Mediterranean sapropels. In particular, it was inferred that

79   persistent ventilation in the Adriatic during the early stage of ~~the~~ sapropel formation hampered the initial

80   development of oxygen-depleted conditions justifying the delayed S1 onset in respect to the rest of the

81   EMS (Mercone et al., 2000; Rohling et al., 2015).

82   This high-resolution (decadal-~~millennial~~centennial) study aims at testing this hypothesis by

83   reconstructing the oceanographic regime under which Adriatic sapropels formed. Our analysis builds on

84   three well-dated sediment cores collected in three different water depths from the shelf to the deep basin

85   (Fig. 1 and 2). With the objective of understanding timing and conditions which promoted anoxic bottom

86   waters, we present a suite of complementary analyses which include foraminifera assemblages, inorganic

87   elemental composition and organic matter composition. The relatively young age of S1 makes it an ideal

88   target to develop a precise radiocarbon-based Bayesian age model across the three sites establishing also a

89   robust chronological link to other S1 ~~depostis~~deposits across the EMS. Thus, by identifying coeval and

90   genetically linked ~~deposits~~strata, we will evaluate the necessary conditions leading to the sapropel S1

91   formation in Adriatic sediments and test to what extent these prerequisites are linked to the deposition of

92   sapropel beds in the rest of the EMS.

93

94   **2. Material and methods**

95   **2.1 Sediment cores**

96   The dataset presented here consists of three piston cores retrieved in the Adriatic Sea with variable

97   barrel lengths (5–20 m) (Fig.1 and 2). Core AMC99-1 (45°51'.80 N & 14°45'.68 E, 260 m; Fig. 1) was

98   collected in the central Adriatic basin from the bottom of the mid-Adriatic depression (MAD, Fig. 2b).

4

99   Core INVAS12-10 (41°30'.25 N & 17°10'.78 E, 570m; Fig 3) and core SA03-1 (41°30'.25 N &

100   17°10'.78 E, 567 m) were collected 5 m apart from each other (i.e., twin cores; Fig. 1 and 2c) in the

101   southwest Adriatic slope. Finally, core ST04-1 (41°27'.46 N & 17°31'.05 E, 1085 m; Fig. 3) was retrieved

102   in the deep basin plain of the south-western Adriatic Sea (Fig. 1 and Fig. 2c).

103

104   **2.2 Seismic acquisition** ~~and core handling~~

105   The seismic dataset used in this study has been collected by ISMAR-CNR (Bologna) on board R/V

106   Urania, in the last two decades. Seismic data were acquired with a hull-mounted Chirp-Sonar Profiler with

107   16 transducers, characterized by 2–7 kHz sweep-modulated bandwidth, equivalent to a 3.5 kHz profiler,

108   with a recording length up to 1500 ms, depending on water depth, and a penetration of 50–100 m, with

109   vertical resolution of ca. 0.5 m. Track line positioning was based on differential GPS navigation, assuring

110   a position accuracy of 10 m and transformed to geographic coordinates referred to the ED-50 datum.

111

112   **2.3 Digital x-ray radiograph**

113   Prior to subsampling, cores were x-rayed using a Gilardoni MPX160 as a source and an amorphous 30 cm

114   long silicon (a-Si) flat panel sensor as a detector (Kodak) typically exposed at 70 kV and 5 mA for ca. 6.4

115   s. For each digital image the pixel dimension is 125 μm and resolution is 1932×2348 pixels.

116

117   **2.~~3~~ 4 Foraminifera**

118   Sediment samples (1-cm thick interval) were oven dried at 50°C, washed through a 63 μm sieve and

119   dried again at 50°C. Each sample was subsequently split into aliquots using a Jones microsplitter. Aliquots

120   were counted to reach at least 300 specimens of planktonic foraminifera and 300 specimens of benthic

121   foraminifera. In anoxic beds only planktonic foraminifera were observed. The quantitative study was

122   performed on the fraction >1~~0~~06~~60~~0μm to avoid juvenile specimens, consistent with the existing Adriatic

123 literature (Favaretto et al., 2008; Narciso et al., 2012; Piva et al., 2008). However, the <1606 μm fraction

124 was always checked in order to identify those specimens which can pass the mesh because of an elongated

125 shape of their shell (e.g. *Fursenkoina*) or because of the small size of their adult stage (e.g. *Epistominella*).

126 ‑Foraminifera concentration is reported as the number of specimens per gram of dry sediment. Data

127 were then integrated with previous published studies (core SA03-1 and AMC99-1; (Favaretto et al., 2008;

128 Narciso et al., 2012; Piva et al., 2008)) to gain higher resolution within the time interval studied.

129 Specifically, twenty-two new samples from SA03-01 were merged with published data (Favaretto et al.,

130 2008; Narciso et al., 2012) while 42 new samples from core AMC99-1 were integrated with data

131 published (Piva, 2007; Piva et al., 2008). Finally, fifty-three samples of core INVAS12-10 were examined

132 with a semi-quantitative analysis to identify key levels (bioevents) for stratigraphic and chronologic

133 purposes (i.e., correlation with the sister core SA03-1), as all geochemical analyses were performed on

134 core INVAS12-10.

135 The Oxygen Index (OI) (Schmiedl et al., 2003) was used to provide a general trend of bottom

136 oxygen conditions. It is calculated as (HO/(HO+LO)+Div) x 0.5 where HO is the relative abundance of

137 high oxygen indicators (Miliolids, *Articulina tubulosa+Cibicidoides pachydermus+Gyroidinoides*

138 *orbicularis*), LO is the relative abundance of low oxygen indicators (*Fursenkoina* spp., *Chilostomella*

139 *oolina*, *Globobulimina* spp.), and Div is the normalized benthic foraminiferal diversity H(S). The term is

140 multiplied by 0.5 to distinguish between anoxic (minimum value = 0) and oxic (maximum value = 1)

141 conditions (Schmiedl et al., 2010; Schmiedl et al., 2003). The index has been calculated for cores ST04-1

142 and SA03-1, while for core AMC99-1 the term LO (=species of the group A by (Jorissen, 1999) with a

143 deep infaunal microhabitat, especially resistant to low oxygen conditions), has been replaced by the

144 infaunal benthonic taxa of the group B by Jorissen (1999), that is *Bolivina* spp/*Brizalina* spp, *Bulimina*

145 *costata/ inflata* and *Uvigerina peregrina*, with an infaunal microhabitat, more opportunistic than the

146 species of group A , but less resistant for low oxygen conditions (Schmiedl et al., 2003) because deep

147 infaunal species were absent, or near-absent, during the time equivalent to the Sapropel 1a deposition, as

already reported in the central Adriatic by Ariztegui et al. (2000). The absence/near-absence of species of the LO term would have resulted into not realistic values indicating highly oxygenated bottom condition in the OI index during the Sapropel 1a interval, making necessary the use of the abundant taxa of group B.

Reworked species used as bottom current proxy include the modern living inner-shelf species such as *Ammonia* spp, *Elphidium* spp, *Haynesina* spp. and epiphyitic species (*Asterigerinata* spp, *Buccella granulata, Patellina corrugata*) (Jorissen, 1988) corresponding to Biofacies II and III in the Adriatic. We interpret the presence of these displaced species by sediment shedding from shallower waters (Trincardi et al., 2007), in particular from outer-shelf coarser/sandy (Spagnoli et al., 2010) deposits formed during the LGM and presently swept by NAdDW. ~~The Oxygen Index (Schmiedl et al., 2003) has been calculated for cores ST04-1 and SA03-1, while for core AMC99-1 the term LO (=low oxygen indicators, corresponding to the deep infaunal benthonic species (Jorissen, 1999)) has been replaced by infaunal benthonic species (*Bolivina* spp/*Brizalina* spp, *Bulimina costata/in*flata and *Uvigerina peregrina*) (Schmiedl et al., 2003) as deep infaunal species were absent.~~ Reworked species used as bottom current proxy include *Ammonia* spp, *Elphidium* spp, and ~~epifitic~~epiphytic species corresponding to Biofacies II and III in Adriatic (Jorissen, 1988). We interpret the presence of these displaced species by sediment shedding from shallower waters (Trincardi et al., 2007), in particular from outer-shelf coarser/sandy (Spagnoli et al., 2010) deposits formed during the LGM and presently swept by NAdDW.

~~Reworked species used as bottom current proxy include the modern living inner-shelf species such as *Ammonia spp, Elphidium spp, Haynesina spp.* and *epifitic* species (*Asterigerinata spp, Buccella granulata, Patellina corrugata*) (Jorissen, 1988) corresponding to Biofacies II and III in the Adriatic. We interpret the presence of these displaced species by sediment shedding from shallower waters (Trincardi et al., 2007), in particular from outer-shelf coarser/sandy (Spagnoli et al., 2010) deposits formed during the LGM and presently swept by NAdDW.~~

Radiocarbon measurements on monospecific tests (5-7 mg) of the planktonic foraminifer *Globigerinoides ruber* (species living above the thermocline) were performed at the National Ocean

Sciences Accelerator Mass Spectrometry (NOSAMS) Facility (USA). On average, 400-600 specimens were hand-picked from the size fraction > ~~0.~~180 ~~µm~~m. Specimens were ultrasonicated in distilled water to remove potential sediment impurities. For level ST040-1 XII 61-62 cm, the planktonic foraminifer *Globorotalia inflata* was used due to the lack of a sufficient amount of *G. ruber* specimens.

2.~~6~~ 5 X-ray fluorescence (XRF)

The inorganic composition of bulk sediments was characterized using a wavelength dispersive sequential Philips PW2400 XRF spectrometer (Mercone et al., 2001) ~~(at the~~ Department of Geosciences, ~~(~~University of Padova). The XRF instrument was operated under vacuum conditions on samples prepared as glass beads using lithium tetraborate and melted with a fluxer Claisse Fluxy (~1150°C). The standard error (based on several measurements of the same sample) is less than 0.6% and 3% for major element and trace elements, respectively. For this study, we focused on selected elements which include Ti, V, Mn and S. ~~. Sediments corresponding to tephra layers (characterized by high Zr excess) were analyzed but the data are not shown.~~

2.~~7~~ 6 Grain-size

About 3 g of dried sediments were resuspended in a 40 ml solution of sodium metaphosphate (0.6%) and sonicated for 20 minutes at high energy. Prior to the analysis, sample~~sd~~ were wet sieved at 63 µm. A few drops of wet samples were checked with the microscope to examine the presence of microfossil remains. ~~P~~Particle size distribution of the <63 µm fraction was measured using a Micromeritics SediGraph™ III 5120~~.~~ according to the settling velocity method (Bianchi et al., 1999). Sortable silt concentration was calculated as the fraction by weight of the total mass ranging between 10 and 63µm (McCave and Hall, 2006).

2.8 7 Organic Geochemistry

Samples for organic carbon (OC) content were placed in silver capsules and pre-treated with HCl (1.5 M) to remove the inorganic carbon (Nieuwenhuize et al., 1994). Oven-dry samples were analysed using a Thermo Quest-Finnigan Delta Plus isotope ratio mass spectrometer, directly coupled to a FISONS NA2000 Elemental Analyzer by means of a CONFLO II interface.

Lignin analyses (terrigenous biomarkers) were carried out using a Microwave digestion system (Tesi et al., 2014). Dry samples were placed in Teflon vessels with 8 ml of alkaline solution (2N NaOH), 500 mg of CuO, 50 mg of $Fe(NH_4)2(SO_4)2\cdot6H_2O$ and oxidized for 1.5 h at 150 °C. After the oxidation, a known amount of recovery standards (ethylvanillin and trans-cinnamic acid) were added to each vessel and acidified to pH 1 with HCl. Reaction products were then extracted with ethyl acetate, evaporated to dryness under N_2 and redissolved in pyridine. Reaction products were analysed as trimethylsilyl derivatives (BSTFA reagent) via GC-MS. Compounds were separated chromatographically in a 30 m×250 μm DB1 (0.25 μm film thickness) capillary GC column, using an initial temperature of 100 °C, a temperature ramp of 4 °C min^{-1} and a final temperature of 300 °C. Phenol biomarkers were quantified using the response factors of commercially available standards (Tesi et al., 2014).

3. Chronology

3.1 Age-depth models

Bayesian age-depth models were performed using the OxCal 4.2 program (https://c14.arch.ox.ac.uk/embed.php?File=oxcal.html) and a comprehensive dataset, which includes both ^{14}C measurements carried out on monospecific foraminifera samples (this study) as well as radiocarbon-dated bioevents based on a detailed event biostratigraphy from each sediment core (Fig. 4 and 5). Radiocarbon age (uncalibrated) of well-known bioevents was based on published studies in the Adriatic (Table 1).

221   Bioevents (uncalibrated) used for the age-depth models include the following planktonic species or

222   planktonic assemblage turnovers (Fig. 4 and Table 1):

223   - Bioevent I (10450±90 ^{14}C yBP), abrupt increase of *Globigerinoides ruber,* a warm-water species

224   ~~signaling~~signalling the top of the Younger Dryas dated in core CM92-43 (Asioli et al., 2001). This

225   bioevent marks the end of the Greenland Stadial 1 (GS1) and the beginning of the Holocene (top ecozone

226   V) (Asioli et al., 2001; Asioli et al., 1999; Blockley et al., 2004) and also the top of ecozone 7 (Siani et al.,

227   2010) . The GS-1/Holocene transition is also testified by the lowering of the δ^{18}O values (Asioli et al.,

228   1999; Jorissen et al., 1993; Narciso et al., 2012; Siani et al., 2000);

229   - Bioevents II and III (9860±60 and 9360±50 ^{14}C yBP, respectively), two peaks in the abundance of

230   *Globorotalia inflata* (i.e., younger and older). These bioevents were described and dated in core SA03-1

231   (Favaretto et al., 2008) before its temporary disappearance at the base of the Sapropel S1;

232   - Bioevent IV (5880±60 ^{14}C yBP), last Occurrence of *G. inflata* dated in core RF93-30 (Trincardi et al.,

233   1996). This is a well-documented bioevent recognized in the whole Adriatic after the sapropel

234   S1termination (Ariztegui et al., 2000; Asioli et al., 1999; Capotondi et al., 1999; Siani et al., 2010).

235   All ^{14}C dates (new radiocarbon dates and bioevents) were converted to calendar years (cal yr BP)

236   using the latest Marine13 calibration curve (Reimer et al., 2013) in OxCal, prior to calibration, ages were

237   corrected for an extra 136±41 ^{14}C-years regional reservoir effect (ΔR) using the values reported in the

238   Marine Reservoir Correction Database (http://calib.qub.ac.uk/marine/). Above the sapropel unit (<5 kyr),

239   the age-depth model of AMC99-1 relays on benthic monospecific tests (*Cibicidoides pachyderma*). For

240   this reason, ~~Only for core AMC99-1 and above the sapropel deposit, ΔR was set 336±41~~ an extra 200

241   years of reservoir correction was used for these ~~for~~ radiocarbon ages *Cibicidoides pachyderma* ~~(benthic~~

242   ~~species) based~~ according to ~~on~~ the ~~difference~~ offset between planktonic and benthonic organisms

243   previously assessed in this core (Piva et al., 2008). Bayesian age-depth model (Lowe et al., 2007; Ramsey,

244   1995; Ramsey and Lee, 2013) was implemented using variable rigidity for the Poisson-Process Modeling

245   (*k* variable ranging between 0.01 and 100 cm^{-1}). The Outlier-Model analysis was performed with the

246   *General setting* and the prior probability fixed to 0.05, which weighs down the radiocarbon measurement

247   that have statistical probability of more than 5% of being outliers. The output resulted in robust age

248   models with an overall solid structure of the dated sequence (Fig. 5) as defined by an excellent agreement

249   index (>90%) between calibrated and modelled ages.

250   It is worth mentioning that foraminifera assemblages were studied in SA03-1 core while the rest of

251   the analyses were performed on the sister core INVAS12-10 from the same site (Fig. 1 and 2c) on which

252   we have constructed the age-depth model based on a greater number of radiocarbon measurements. Cross-

253   correlation between twin cores was carried out relaying on bioevents and tephra (magnetic susceptibility

254   anomalies). Events in chronological order include: top of the Younger Dryas, two *G. inflata* peaks (during

255   the Pre Boreal), peak of *C. bradyi*, a large magnetic susceptibility peak marking a tephra layer, two *G.*

256   *inflata* peaks (during S1 break and S1b, respectively) and the Last Occurrence of *G. inflata* (Fig. 4). Ages

257   between midpoints were estimated via linear interpolation.

258

259   **3.2. Comparison between stratigraphic records from the southern Adriatic basin**

260   Prior studies have investigated the S1 in the southern Adriatic basin in the following cores: IN68-9

261   (Jorissen et al., 1993; Rohling et al., 1997; Van Straaten, 1970), MD90-197 (Mercone et al., 2001;

262   Mercone et al., 2000; Siani et al., 2013; Siani et al., 2000; Siani et al., 2010) and AD91-17 (Capotondi et

263   al., 1999; Giunta et al., 2003; Sangiorgi et al., 2003) (Fig. 6A). Here, prior to presenting and discussing the

264   data, we compare our record from the same region with these published records from the stratigraphic

265   point of view. For the comparison, we selected five main widespread bioevents commonly observed in the

266   Adriatic Sea (Fig. 6B) (Asioli et al., 1999; Narciso et al., 2012; Piva et al., 2008; Rohling et al., 1997;

267   Santacroce et al., 2008; Trincardi et al., 1996). Bioevents include:

268   - bioevent I (top GS-1/YD): abrupt increase of *G. ruber*

269   - bioevent II: older peak of *G. inflata*

270   - bioevent III: younger peak of *G. inflata*

271   - *G. ruber* maximum peak of frequency in S1a

272   - *Globoturborotalita rubescens* peak in S1a

273

274   Among these cores, IN68-9 core (i.e., core 362 in previous publications (Van Straaten, 1970) is

275   particularly relevant because our current understanding of the S1 onset is largely based on this record

276   (Rohling et al., 1997; Rohling et al., 2015). IN68-9 was collected at 1234 m water depth (Fig. 11A) and all

277   the aforementioned biostratigraphic events (source PANGEA, doi:10.1594/PANGAEA.407648) are

278   present and stratigraphically coherent with ST04-1 (bioevent I corresponds in this core to the ecozones I/II

279   boundary) (Fig. 6B). Another similarity includes the ash layer at cm 128-130. Geochemical analysis

280   defined this event as Mercato tephra (Calanchi and Dinelli, 2008) which is positioned just below the

281   increase of *G. rubescens*.

282   Despite the overall coherence between IN68-9 and ST04-1 from a stratigraphy point of view,

283   bioevents in IN68-9 exhibit a much younger age compared ST04-1, especially within S1a. To further

284   investigate this discrepancy, we performed a new picking of planktonic foraminifera directly on IN68-9

285   close to the *G. ruber* peak (137-138 cm). It was possible to date this interval in core IN68-9 because two-

286   thirds of the original core are currently stored at ISMAR Bologna. The new radiocarbon date (9030±30 yr

287   BP, uncalib.; NOSAMS-WHOI; Table S1) turned out much older than the age assessed with the previous

288   age-depth model (ca. 8110 yr BP ^{14}C age) but remarkably consistent with the chronology of ST04-1.

289   The reason for this offset (ca. 1000 y) between the new radiocarbon date and the previous age-depth

290   model (Rohling et al., 1997) is unknown and falls outside the scope of this manuscript. However, it is

291   worth mentioning that the age-depth model of IN68-9 within the S1 interval essentially relies only on two

292   radiocarbon dates (Rohling et al., 1997). We can only suppose that the problem might derive from the

293   lowest radiocarbon date (155.5-157.5 cm, 9280±180 yBP ^{14}C) which is somehow erroneously too young.

294   In fact, this interval roughly corresponds to bioevent II which is again much younger (ca. 1000 years)

295   when compared with our record. Furthermore, this offset is conservative considering that this radiocarbon

296 test at 155.5-157.5 cm corresponds to a mixture of benthic foraminifera (Jorissen et al., 1993). Thus, at

297 most, the radiocarbon date should have been older rather than younger.

298 Core MD90-197 was collected at 1010 m water depth (Fig. 6A). Three curves of planktonic species

299 (*G. ruber*, *G. inflata* and *Globigerinita glutinata*) were visually extrapolated based on the plot of

300 planktonic species *vs* age previously published (Siani et al., 2010). For this core only two bioevents of

301 core ST04-1 were recognized: Bioevent I and II. The *G. ruber* peak is present but it is coeval with the

302 tephra layer E1 (Gabellotto-Fiumebianco) located close to the S1 interruption and proved to be younger

303 than Mercato tephra (Caron et al., 2012; Marchini et al., 2014). What is striking about this core is the

304 relatively lower thickness of S1a compared to S1b which is unusual for S1 (Mercone et al., 2001; Mercone

305 et al., 2000). This might reflect either a condensed interval or a hiatus above the *G. glutinata* peak. To test

306 this hypothesis, we compared the V/Al record that displays a large peak right after the S1 onset in both

307 Adriatic basin (ST04-1) and slope (INVAS12-10) (Fig 6C). This peak is also well present in other south-

308 eastern S1 deposits (e.g., LC21, Aegean Sea (Mercone et al., 2001). The XRF analyses were performed

309 every cm in MD90-197. However, despite the high resolution, the V/Al peak is not visible (Mercone et al.,

310 2001) (Fig. 12C)

311 An examination of all radiocarbon dates available for MD90-197 (both mixed planktonic

312 foraminifera and monospecific tests (Mercone et al., 2000) reveals a drastic drop in sedimentation rate

313 where the V/Al is expected. This suggests once again either a condensed unit or a hiatus. Even considering

314 the error associated with pulling together monospecific radiocarbon tests and mixed planktonic species

315 (these latter integrate the signal of a thicker water column), the apparent drop of sedimentation seems to

316 be still evident in the radiocarbon data (Mercone et al., 2000). Unfortunately, benthic foraminifera are not

317 available for MD90-197 which hampers the direct comparison with ST04-1. For example, the *C. bradyi*

318 observed in both ST04-1 and IN68-9 at the base of S1a could have provided additional important clues.

319 Finally, core AD91-17 was collected at 844 m water depth. Two curves of planktic foraminifers (*G. ruber*

320 and *G. inflata*) were reported in Fig. 6A based on previous studies (Capotondi et al., 1999). A recent study

13

321 showed that the Mercato tephra in this core is present in correspondence of the S1 onset (Marchini et al.,

322 2014). However, Mercato is stratigraphically positioned ca. in the middle of S1a above the *G. ruber* peak

323 in both IN68-9 and ST04-1, this implies that the lower part of S1a is not present. Indeed, just below

324 Mercato, previous publications have highlighted the presence of a turbidite (Giunta et al., 2003).

325

326 Finally, core AD91-17, collected at 844 m water depth (6A), records the Sapropel 1 deposition between

327 cm 190 and 125 (Giunta et al., 2003, Marchini et al., 2014). Two curves of planktic foraminifers (G. ruber

328 and G. inflata) were reported in Fig. 6A based on previous studies (Capotondi et al., 1999).

329 Tephrostratigraphy of this core shows that the sapropel onset (190-191 cm) corresponded to upper limit of

330 Mercato tephra (Marchini et al., 2014). However, Mercato tephra is stratigraphically positioned ca. in the

331 middle of S1a, above the *G. ruber* peak in IN68-9 (Calanchi and Dinelli, 2008; Rohling et al., 1997) and

332 in ST04-1. The fact that this *G. ruber* positioned peak below Mercato is not visible in AD91-17 (Fig. 6A)

333 suggests that the lower portion of the S1a is missing. In fact, previous publications have highlighted the

334 presence of a turbidite just below Mercato between cm 200 and 196 (Giunta et al., 2003) which further

335 support the hypothesis of the stratigraphic gap.

336

4. Results and discussion

4.1 Coeval sapropel deposits cross-margin settings

In this study we present data from sediment cores retrieved in three different regions of the Adriatic Sea: (i) the mid-Adriatic depression (MAD), (ii) the south-western continental slope and (iii) the southern deep basin (Figs. 1 and 2). The mid-Adriatic depression represents a small remnant basin, which was partially filled with sediment during the last glacial maximum (core AMC99-1, 260 m (Piva et al., 2008); Fig. 2b). High-resolution chirp-sonar profile across the coring site shows continuous and high-amplitude sub-parallel reflectors, which denote sedimentation in low-energy conditions.

345   The slope coring site is characterized by large-scale bottom-current deposits formed by prolonged

346   activity of the thermohaline circulation (core INVAS12-10 and SA03-1, from 570 and 567 m respectively

347   (Minisini et al., 2006) (; Fig. 2c). On chirp profiles, these deposits are organized in fields of large sediment

348   waves characterized by wavy and high-amplitude reflectors (Fig. 2c). The coring site was selected on the

349   depositional (up-current) flank of one sediment wave.

350   Finally, the coring site in the southern Adriatic deep basin is characterized by pelagic

351   sedimentation as shown by sub-parallel reflectors, although dense NAdDW can occasionally reach and

352   impact this area (ST04-1, 1085 m Minisini et al. (2006); Fig. 2d).

353   Despite the different bathymetric contexts, radiocarbon dates from monospecific tests indicated

354   that these three records represent coeval deposits within the time interval under examination (Table 1).

355   Detailed biostratigraphy examination for all three cores revealed the occurrence of bioevents commonly

356   observed in the study region, which were used to independently test the stratigraphic continuity of our

357   records (Fig. 4). High-resolution Bayesian ^{14}C-based age-depth models confirmed continuous deposition

358   consistent with bioevents and seismic profiles (Fig. 5).

359

360   **4.2 Adriatic Sapropel deposition**

361   **4.2.1 Pre-sapropel and S1 onset**

362   Sapropels are beds with elevated organic carbon (OC) content that contrast with overlying and

363   underlying sediments. In this study, S1 boundaries are defined based on the OC anomalies in respect to the

364   background level. The definition of sapropels can further extend to anomalies of several other parameters

365   including Ba/Ti ratio, redox sensitive elements, foraminifera assemblages and magnetic susceptibility or

366   simply changes in sediment colour (De Lange et al., 2008; Mercone et al., 2000; Rohling et al., 1997;

367   Santvoort et al., 1997; Schmiedl et al., 2010; Tachikawa et al., 2015; Vigliotti et al., 2008). Here, we will

368   also discuss these other parameters alongside along the OC data in order to provide a multifaceted view on

369   S1 formation.

370   Our deepest ~~water~~ record ~~in~~ from the southern Adriatic (ST04-01, 1085 m; Fig. ~~7a~~6a) shows a

371   gradual OC increase since 11 cal. ky BP before the typical sapropel onset (ca. 10 cal. ky BP) (Hennekam

372   et al., 2014; Rohling et al., 2015; Schmiedl et al., 2010). This trend is consistent with the foraminifera-

373   based oxygen index (Schmiedl et al., 2010) (OI) which reveals a pre-sapropel deterioration of ~~pore-~~

374   ~~water~~bottom oxygen levels in the deep basin since ca. 11 cal. ky BP (Fig. ~~8a~~7a and Fig. ~~9a~~8a). Analogous

375   pre-sapropel conditions, ascribed to stratification have recently been documented in the deep Levantine

376   basin at 1780 m water depth using a suite of redox-sensitive elements (Tachikawa et al., 2015). Post-

377   glacial freshening driven by the inflow of less saline Atlantic waters via the Gibraltar strait followed by

378   the African Humid Period have certainly exerted a major control on the surface water stratification,

379   vertical mixing and hence intermediate and deep water formation (Rohling et al., 2015; Weldeab et al.,

380   2014). ~~(Rogerson et al., 2008)~~This is ~~also~~ in line with recent regional simulations which described a

381   gradual deterioration of the deep water ventilation in the EMS since the Heinrich-1 event (H1, ca. 18-16

382   cal ky BP) (Grimm et al., 2015). Enhanced stratification since the H1 event was one of the major drivers

383   that promoted the formation of organic rich layers (ORLs) in the Alboran Sea (Rogerson et al., 2008). In

384   this western Mediterranean region, the continental run-off due to Alpine glacier thawing (i.e., enhanced

385   Rhone river discharge) combined with the Atlantic inflow likely weakened the Western Mediterranean

386   Deep Water ventilation promoting the deposition of ORLs (Rogerson et al., 2008).

387   The onset of relatively high OC content which marks the beginning of the Adriatic S1 (i.e, S1a)

388   was synchronous among our records and it was dated around 10 cal ky BP ~~in~~ across the ~~all~~ three sites (Fig.

389   ~~7~~6 a, b, c). After this coeval OC increase, the deep Adriatic basin (ST04-1) rapidly turned into an azoic

390   environment (Fig. ~~9a~~8a). Specifically, as the pore water oxygen decreased in the basin (Fig. 8a), only

391   infaunal foraminifera could initially tolerate oxygen-poor conditions although the benthic environment

392   rapidly became hostile even for deep infaunal taxa (Fig. ~~9b~~8b). Azoic conditions in the basin are marked

393   also by authigenic vanadium enrichments (V/TiO$_2$; Fig. ~~9b~~8b) as commonly observed in sapropel beds

394   (Mercone et al., 2001; Tachikawa et al., 2015). Vanadium precipitation is expected in highly reducing

395   environments as its solubility rapidly decreases at the oxic-anoxic boundary which is controlled via

396　diffusion processes across the sediment-water interface (Mercone et al., 2000). Sulphur enrichment

397　(S/TiO$_2$) in sapropel beds - likely in the form of authigenic pyrite (Passier et al., 1997) - further

398　corroborates the change of redox conditions characterized by microbial-driven sulfate reduction in

399　response to the oxygen-poor environment (Fig. 10 9 d, e, f).

400

4.2.2 Sapropel break, sapropel S1b and sapropel termination

402　An interruption within the sapropel unit is visible in our records between ca. 7.8 and 8.3 cal ky

403　BP. During the break both OC content and V/TiO$_2$ decreased while the OI increased indicating a

404　temporary re-oxygenation at the seabed (Fig 7a 6a, b, c; Fig 8 7). The overall trend observed here has been

405　documented in several other S1 deposits further south-east and down to ca. 1,800 m water depth (De

406　Lange et al., 2008; Tachikawa et al., 2015). Reactivation of the convective overturn driven by heat loss

407　during cooling events in the northern Adriatic has been suggested as the most likely scenario to explain

408　the temporary re-oxygenation (Marino et al., 2009; Rohling et al., 1997). The interruption was particularly

409　evident over basin and slope sediments while in the shallower mid-Adriatic slope basin did not display

410　significant change over the break. Already being an oxic environment, it is likely that the mid-Adriatic

411　depression (AMC99-1) was not particularly affected by the temporary resumption of the ventilation.

412　After the sapropel break, the second phase of S1 deposition (i.e., S1b) lasted for ca. 1 ky. Both

413　V/Ti ratio and oxygen index indicate that the reducing conditions during S1b were not as severe in slope

414　sediments as during S1a (Fig. 8 7 c, d). This is also consistent with the presence of relatively lower

415　authigenic sulphur content, which suggests comparatively lower sulphate reduction rates during S1b (Fig.

416　10 9 d, e, f). By contrast, the deep southern basin became azoic again for ca. 500 yr (Fig. 8a 7 a and 8 a).

417　The transitory reappearance of benthic foraminifera and high OI value around 7.4 cal ky BP in the

418　deep basin (ST04-1) suggests another short-lived ventilation event within the S1b (Fig. 7 8a) prior to the

419　S1 termination. This was a rather short-lived event but widespread over the EMS as previously observed

420　in the Aegean and Ionian regions (Filippidi et al., 2016).

17

421   The complete recovery of the deep-water ventilation, which marks the sapropel termination, was

422   fairly synchronous among our records according to the OC anomalies (ca. 6.8 cal ky BP, Fig. 7 6 a,b,c).

423   However, the OI displayed a bathymetric gradient (Fig. 8a7a, b, c) consistent with what observed in the

424   Levantine and Aegean regions where the ventilation started in shallow environment and gradually

425   extended towards greater water depths towards deeper sediments (Schmiedl et al., 2010). As the oxygen

426   reached the seabed, the authigenic enrichment of MnO_2 (Fig. 10a9a) provides a geochemical redox marker

427   to track the maximum penetration of oxygen in sediments after the anoxic period (Reitz et al., 2006;

428   Tachikawa et al., 2015).

429   While OC concentration levels were re-established after the sapropel over basin and slope, the

430   OC remained relatively high in the mid-Adriatic depression (AMC99-1; Fig. 7 6 c) even after the S1

431   termination. The OI based on intermediate infaunal foraminifera reveals a relatively moderate but

432   continuous decrease of the pore-water oxygen concentration in this region throughout the S1 deposition

433   (Fig. 8c7c). This trend likely reflected the sea level rise which pushed towards land the main path of the

434   North Adriatic Deep Water (NAdDW) causing a less efficient ventilation of the Adriatic depression. It is

435   well documented that the modern NAdDW path is mainly confined to the western shelf due to the Coriolis

436   force as it moves southwards (Vilibić and Supić, 2005). Today, only major events of dense water

437   formation can efficiently ventilate the deepest region of the Adriatic depression (Marini et al., 2015).

438   When this occurs, the dense plume lifts the old water mass which is characterized by relatively low

439   oxygen concentrations testifying its long residence time within the morphological depression (i.e., one or

440   several years) (Marini et al., 2015).

441

442   **4.3 Sediment waves growth and thermohaline forcing**

443   In the South Adriatic slope within the field of upslope-migrating sediment waves (core SA03-1,

444   567 m; Fig. 2c), the relative abundance of reworked inner-shelf foraminifera suddenly decreased at the S1

445   onset (Fig. 67d). The presence of allochthonous taxa at this depth is expected considering the

446 thermohaline forcing that generates these sedimentary bodies (Trincardi et al., 2007). Specifically,

447 sediment waves are essentially swept by protracted thermohaline currents which have sufficient energy to

448 resuspend inner-shelf taxa and disperse them towards greater depths (Langone et al., 2015). Bottom

449 currents in the southern Adriatic slope are principally controlled by LIW and NAdDW as well as their

450 interaction which ultimately generates the Adriatic Eastern Mediterranean Deep Water (EMDW$_{Adriatic}$)

451 (Millot, 1999). Mooring lines deployed just down-flow respect to the sediment wave field showed that the

452 modern NAdDW-driven bottom currents can reach over 60 cm s^{-1} during the cascading season (Langone

453 et al., 2015) (i.e., the modern NAdDW forms around Jan-Feb and reaches the southern margin around

454 March-April (Langone et al., 2015; Turchetto et al., 2007). Consequently, the sudden decrease of inner-

455 shelf taxa coeval with the S1 onset likely reflects the virtual shutdown of the NAdDW or, more precisely,

456 a shallow ventilation confined to the uppermost region of the water column.

457 This explanation is indeed consistent with the general temporal trend shown by the shedding of

458 allochthonous foraminifera from the shelf throughout the S1 deposition. For example, as previously

459 mentioned, the S1 interruption is likely the expression of a cooling phase which promoted the temporary

460 reactivation of the dense water formation in the northern Adriatic Sea (Rohling et al., 1997) and,

461 consequently, the advection of reworked inner-shelf taxa over the slope (Fig. 7d6d). Likewise, S1b and S1

462 termination are associated with decrease and increase of inner-shelf taxa, respectively (Fig. 7d6d).

463 The non-cohesive fraction of marine sediments - generally known as ''sortable silt'' (SS, 10–63

464 μm) - further supports the decrease of the deep-water ventilation during the S1 deposition (Fig. 7e6e). The

465 sortable silt is operationally defined as the fraction of fine-grained sediments whose sorting and

466 concentration vary in response to hydrodynamic processes (McCave and Hall, 2006). As large errors

467 affect the SS mean grain estimates for low concentrations of SS, here we report only the SS% by weight

468 as a qualitative proxy for paleo-current regimes (Fig. 7e6e). The SS% suggests a progressive decrease of

469 the bottom-current energy since the end of the Younger Dryas (ca. 11.5 cal ky BP) with the minimum

470 observed just at the S1 onset. Overall, the SS trend is consistent with the general distribution of the inner-

471 shelf foraminifera (Fig. ~~7d~~6d), which further highlights drastic changes of the thermohaline forcing

472 associated with the pace of the NAdDW.

473

474 **4.4 Weakening of LIW as main trigger for Adriatic S1 deposits**

475   Our results from the sediment wave field revealed that the onset of the sapropel S1 in Adriatic

476 sediments is coeval with the drastic weakening of the North Adriatic Deep Water (NAdDW, Fig. 1).

477 Based on this evidence, we envision a direct relation of cause and effect in which suddenly weakened

478 deep water ~~ventilation~~ formation resulted in oxygen depleted bottom waters.

479   Several combined factors might have caused the abrupt decrease of the thermohaline forcing in

480 the Adriatic Sea. A key aspect to consider lies in the evident similarities with the south-eastern

481 Mediterranean Sea. First of all, the comparison with the Levantine, Aegean and Ionian Seas reveals that

482 the S1 onset in the Adriatic is ~~remarkably~~ coeval (within age-depth model uncertainties) with the sapropel

483 formation in these regions. Specifically, a recent review (Schmiedl et al., 2010) that has compiled several

484 south-eastern Mediterranean cores indicated that the onset of critical oxygen concentrations (i.e, oxygen

485 index being less than 0.5) occurred around 10.2±0.3 cal ky BP. The collapse of the Adriatic benthic fauna

486 in slope and basin sediments based on the same oxygen index threshold occurred within this time interval

487 (Fig. ~~8~~10 ~~a, b~~). This comparison thus reveals that S1 onset in the Adriatic was coeval with the rest of the

488 south-eastern Mediterranean sapropel beds. Further evident similarities ~~with the south-eastern~~

489 ~~Mediterranean sapropels~~ emerge when comparing the temporal anomalies of several other geochemical

490 parameters such as bulk OC (Filippidi et al., 2016; Hennekam et al., 2014; Vigliotti et al., 2011) and

491 redox-sensitive elements (Filippidi et al., 2016; Hennekam et al., 2014; Mercone et al., 2001; Tachikawa

492 et al., 2015) (notably vanadium).

493   ~~A synchronous S1 onset across the entire EMS – including the Adriatic - is a new element that~~

494 ~~corrects previous literature which inferred a delayed S1 onset of ca. 1ky in the Adriatic due to protracted~~

495 ~~ventilation during the early phase of the sapropel formation (Rohling et al., 1997). In the 3.2 section~~

496 ~~(Comparison between stratigraphic records from the southern Adriatic basin) we have further analysed the~~
497 ~~differences between our results and previous published studies from a stratigraphic point of view. Here we~~
498 ~~show how time differences are most likely the result of low-resolution age-depth models combined with~~
499 ~~gravity-driven processes (e.g., erosion, turbidites) which likely altered the original stratigraphy.~~

500   In light of this new ~~new~~ insight~~information~~, we postulate that the synchronous onset of sapropel
501 S1 over the entire EMS (Fig. 10) necessarily involves the Levantine Intermediate Water (LIW) (Fig. 1~~2~~)
502 which is the binding element of the eastern Mediterranean thermohaline circulation (Millot, 1999). More
503 specifically, we suggest that the most plausible scenario to explain (i) the coeval S1 onset and (ii) the
504 sudden weakening of the NAdDW must be related to the freshening of the south-eastern Mediterranean
505 Sea. According to our hypothesis, because the salty LIW exerts first-order control on the NAdDW
506 formation by pre-conditioning the northern Adriatic waters (Vilibić and Orlić, 2002; Vilibić and Supić,
507 2005) before the winter cooling, we infer that the freshening of the Levantine Sea during the African
508 Humid Period ~~–~~must have considerably reduced the deep-water formation in the northern Adriatic Sea
509 eventually leading to the deep-water anoxia ~~(Fig. 12b)~~.

510   To test our hypothesis ~~(Fig. 12b)~~ and in particular the link between the south-eastern
511 Mediterranean region and Adriatic Sea, we have compared our data with a recent reconstruction of the
512 Nile River discharge based on the Ba/Ca ratio measured on *Globigerinoides ruber* (Weldeab et al., 2014)
513 (Fig. ~~7~~6f). The Ba/Ca record essentially reflects the degree of the freshening of the Levantine surface
514 waters as a function of the African monsoon extent (Weldeab et al., 2014). We found that the maximum
515 freshwater supply to the Levantine Sea (ca. 10 cal ky BP) indeed corresponds to the temporarily NAdDW
516 shutdown (i.e., drop in the inner-shelf taxa and SS, Fig. ~~7~~6 d, e) and the corresponding S1 onset in the
517 Adriatic Sea (Fig. ~~7~~6 a, b, c and ~~8~~7 a, b, c).

518   Furthermore, considering that the formation of the ~~Adriatic~~ Eastern Mediterranean Deep Water
519 sourced from the Adriatic ~~EMDW~~ (EMDW$_{Adriatic}$) largely depends on the NAdDW (Vilibić and Orlić,
520 2002; Vilibić and Supić, 2005) (Fig. 1), our results imply that the reduced deep water formation in the

Adriatic had in turn drastically hampered the ventilation of those deep regions under the direct influence of the EMDW$_{Adriatic}$ which today such as the Ionian basin (Fig. 12b). Today the Adriatic represents the major cold and EMDW dense water source of for the EMS (Klein et al., 2000). although under certain climate conditions (commonly known as the Eastern Mediterranean Transient, EMT), the south-eastern surface waters can become particularly salty and generate large volumes of dense water (Lascaratos et al., 1999; Malanotte-Rizzoli et al., 1997). The EMS freshening certainly had important effects on both NAdDW and EMT.

Recent studies have also pointed out that that the progressive stagnation of the EMS occurred prior to the African Humid Period due to the inflow of less saline North Atlantic waters into the Mediterranean via the Gibraltar strait (Béthoux and Pierre, 1999; Grimm et al., 2015; Rohling and Bryden, 1994; Rohling et al., 2015). Therefore, the peak of the African monsoon occurred over a period already characterized by enhanced water-column stratification. Evidence of weakened deep-water ventilation prior to S1 has been well documented in the Levantine Basin (Tachikawa et al., 2015)[15], which is consistent with our record in the Adriatic basin (notably ST04-1; Fig. 98). The presence of pre-sapropel conditions in our deepest record further highlights the coherence between the Adriatic and the rest of the EMS as well as the importance of pre-freshening as a prerequisite for the sapropel formation (Grimm et al., 2015).

Among other relevant similarities with the south-eastern Mediterranean sapropels, it is worth mentioning that the S1 termination in the Adriatic was coherent with the progressive reoxygenation observed in the Levantine and Aegean sediments (Fig. 10). Specifically, according to the foraminifera-based oxygen index (values > 0.5) (Schmiedl et al., 2010) in these regions, the ventilation was initially confined within the uppermost water column and gradually increased water depth with time. A similar water depth- trend characterized our Adriatic records. Using the same oxygen-index threshold as for the Aegean and Levantine basins (Schmiedl et al., 2010), the re-oxygenation over the slope (SA03-1, Fig. 8b7b and 10) occurred much earlier than the deep benthic environment (ST04-1, Fig. 8a7a and 10). In line with the bottom- current proxies (Fig. 7 6 d, e), these results suggest a gradual reactivation of the

Comment [TT1]:

546 NAdDW. The reason for the observed bathymetric trend across all Eastern Mediterranean basins probably

547 involves the gradual weakening of the African monsoons (Weldeab et al., 2014) (Fig. 7f6f) coupled with

548 the sea surface cooling towards the end of the sapropel (Marino et al., 2009; Siani et al., 2013).

549

550 **4.5 Comparison with published stratigraphic records from the southern Adriatic basin**

551 Our results revealed Aa synchronous S1 onset across the entire EMS which —includes ing the

552 Adriatic setting. This is a new element that corrects previous literature which inferred a delayed S1 onset

553 (of ca. 1ky) in the Adriatic due to protracted ventilation during the early phase of the sapropel formation

554 (Rohling et al., 1997). In the 3.2In this section, we revisit published studies dealing with the Adriatic S1 to

555 evaluate the stratigraphic coherence with our results and, thus, further understand the origin of this

556 discrepancy. section (Comparison between stratigraphic records from the southern Adriatic basin) we have

557 further analysed the differences between our results and previous published studies from a stratigraphic

558 point of view. Here we show how time differences are most likely the result of low-resolution age-depth

559 models combined with gravity-driven processes (e.g., erosion, turbidites) which likely altered the original

560 stratigraphy.

561 Prior Adriatic studies focused on the following cores: IN68-9 (Jorissen et al., 1993; Rohling et al.,

562 1997; Van Straaten, 1970), MD90-197 (Mercone et al., 2001; Mercone et al., 2000; Siani et al., 2013;

563 Siani et al., 2000; Siani et al., 2010) and AD91-17 (Capotondi et al., 1999; Giunta et al., 2003; Sangiorgi

564 et al., 2003) (Fig. 1 and 11). For the comparison with our records, we selected five main widespread

565 bioevents commonly observed in the Adriatic Sea (Fig. 11) (Asioli et al., 1999; Narciso et al., 2012; Piva

566 et al., 2008; Rohling et al., 1997; Santacroce et al., 2008; Trincardi et al., 1996). Bioevents include:

567 - bioevent I (top GS-1/YD): abrupt increase of *G. ruber*

568 - bioevent II: older peak of *G. inflata*

569 - bioevent III: younger peak of *G. inflata*

570 - *G. ruber* maximum peak of frequency in S1a

571   *- Globoturborotalita rubescens* peak in S1a

572   Among these cores, IN68-9 core (i.e., core 362 in previous publications (Van Straaten, 1970) is

573 particularly relevant because our current understanding of the S1 onset is largely based on this record

574 (Rohling et al., 1997; Rohling et al., 2015). IN68-9 was collected at 1234 m water depth (Fig. 11a) and all

575 the aforementioned biostratigraphic events (source PANGEA, doi:10.1594/PANGAEA.407648) are

576 present and stratigraphically coherent with ST04-1 (bioevent I corresponds in this core to the ecozones I/II

577 boundary) (Fig. 11a). Another similarity includes the ash layer at cm 128-130. Geochemical analysis in

578 IN68-9 defined this event as Mercato tephra (Calanchi and Dinelli, 2008) which is positioned just below

579 the increase of *G. rubescens*. Although the geochemical fingerprint is not available for ST04-1, the age

580 and the stratigraphic position suggest that this ash layer is likely Mercato tephra.

581   Despite the overall coherence between IN68-9 and ST04-1 from a stratigraphy point of view,

582 bioevents in IN68-9 exhibit a much younger age compared to ST04-1, especially within S1a. To further

583 investigate this discrepancy, we performed a new picking of planktonic foraminifera directly on IN68-9

584 close to the *G. ruber* peak (137-138 cm). It was possible to date this interval in core IN68-9 because two-

585 thirds of the original core are currently stored at ISMAR Bologna. The new radiocarbon date (9030±30 yr

586 BP ^{14}C age.; NOSAMS reference OS-127850; Table 1) turned out much older than the age assessed with

587 the previous age-depth model (ca. 8110 yr BP ^{14}C age) (Rohling et al., 1997) but remarkably consistent

588 with the chronology of ST04-1.

589   The reason for this offset (ca. 900 y) between the new radiocarbon date and the previous age-depth

590 model (Rohling et al., 1997) might explain why the Adriatic sapropel S1 exhibited a delayed onset. It is

591 worth mentioning that the age-depth model of IN68-9 within the S1 deposit, essentially relies only on two

592 radiocarbon dates (Rohling et al., 1997). Thus, it possible that the problem might derive from the lowest

593 radiocarbon date (UTC-501, 155.5-157.5 cm, 9280±180 yr BP ^{14}C) which is somehow erroneously too

594 young. To test this hypothesis, we re-modelled in Oxcal the sediment accumulation of core IN68-9 using

595 the new radiocarbon date (OS-127850) and the bioevents as used in our records (supplementary material).

The goal of this exercise was to examine the agreement between the model (*prior*) and the observational data (*likelihood*) which is quantitatively expressed with the "agreement index". As expected, test UTC-501 exhibited a low agreement index and, thus, turned out being an outlier. Furthermore, the agreement index would further decrease considering that the suspicious radiocarbon test (UTC-501) corresponds to a mixture of benthic foraminifera (Jorissen et al., 1993). In fact, if we applied a larger ΔR respect to planktonic foraminifera, the new reservoir correction would make the calibrated age even younger and, thus, less coherent with the rest of the dates.

Core MD90-197 was collected at 1010 m water depth (Fig. 1). Three curves of planktonic species (*G. ruber*, *G. inflata* and *Globigerinita glutinata*) were visually extrapolated based on the plot of planktonic species *vs* age previously published (Siani et al., 2010). For this core only two bioevents of core ST04-1 were recognized: Bioevent I and II. The *G. ruber* peak is present but it is coeval with the tephra layer E1 (Gabellotto-Fiumebianco) located close to the S1 interruption and proved to be younger than Mercato tephra (Caron et al., 2012; Marchini et al., 2014). What is striking about this core is the relatively thin S1a compared to S1b which is unusual for S1 (Mercone et al., 2001; Mercone et al., 2000). This might reflect either a condensed interval or a hiatus above the *G. glutinata* peak. To test this hypothesis, we compared the V/Al record that displays a large peak right after the S1 onset in both Adriatic basin (ST04-1) and slope (INVAS12-10) (Fig 11b). This peak is also present in other south-eastern S1 deposits (e.g., LC21, Aegean Sea (Mercone et al., 2001). The XRF analyses were performed every cm in MD90-197. However, despite the high resolution, the V/Al peak is not visible (Mercone et al., 2001) (Fig. 11b). An examination of all radiocarbon dates available for MD90-197 (both mixed planktonic foraminifera and monospecific tests (Mercone et al., 2000) reveals a drastic drop in sedimentation rate where the V/Al is expected. This suggests once again either a condensed unit or a hiatus. Even considering the error associated with pulling together monospecific radiocarbon tests and mixed planktonic species (these latter integrate the signal of a thicker water column), the apparent drop of sedimentation seems to be still evident in the radiocarbon data (Mercone et al., 2000). Unfortunately, benthic foraminifera are not

621 available for MD90-197 which hampers the direct comparison with our record. For example, the *C. bradyi*

622 observed in both ST04-1 and IN68-9 at the base of S1a could have provided additional important clues.

623   Finally, core AD91-17 was collected in the southern Adriatic at 844 m water depth (Giunta et al.,

624 2003, Marchini et al., 2014). Two curves of planktonic foraminifera (G. ruber and G. inflata) were

625 reported in Fig. 1 based on previous studies (Capotondi et al., 1999). Tephra-stratigraphy of core AD91-17

626 indicates that the reconstructed sapropel onset (190-191 cm) corresponded to the uppermost limit of

627 Mercato tephra (Marchini et al., 2014). However, Mercato tephra is stratigraphically positioned ca. in the

628 middle of S1a, above the *G. ruber* peak in both IN68-9 (Calanchi and Dinelli, 2008; Rohling et al., 1997)

629 and ST04-1 (this study). The fact that this large *G. ruber* peak below Mercato is not visible in AD91-17

630 (Fig. 11a) suggests that the lower portion of the S1a is missing. In fact, previous publications have

631 highlighted the presence of a turbidite just below Mercato between cm 200 and 196 (Giunta et al., 2003)

632 which further support the hypothesis of a possible stratigraphic gap.

633

634

635 **4.65 Enhanced primary productivity or diagenetic signal?**

636   Alternatively, the deposition of the Adriatic sapropel could have been an expression of the high-

637 nutrient supply via freshwater discharge. Under these circumstances, the increased demand of benthic

638 oxygen, necessary to degrade the freshly deposited marine phytodetritus, eventually resulted in anoxic

639 sediments.

640   In this study, we used lignin – the second most abundant macromolecule on Earth after cellulose –

641 as a tracer of freshwater discharge because it has been shown that terrestrial organic biomarkers (notably

642 sediment-normalized concentrations) increase during sapropel deposition (Bouloubassi et al., 1999;

643 Gogou et al., 2007) (Fig. 1112). In northern Mediterranean borderlands, the abundancethis evidence of

644 terrestrial biomarkers has been widely used to infer the link between enhanced freshwater supply and

645 sapropel formation (Bouloubassi et al., 1999; Gogou et al., 2007). Indeed, our results show that lignin

26

646   increased at the S1 onset but, ~~in all settings~~ at the same time, the lignin content markedly diminishes with

647   decreasing water depth (Fig. ~~11~~12). While previous studies mainly drawn their conclusions based on deep

648   sapropel beds (Bouloubassi et al., 1999; Gogou et al., 2007), in this study we took the opportunity to focus

649   also on shallow water equivalent deposits which revealed this water depth trend. However, ~~A~~a pattern like

650   this is~~ ~~ unexpected because typically lignin concentration diminishes with increasing distance from the

651   river outlets in all modern continental margins, including the Adriatic (Bröder et al., 2016; Gordon and

652   Goñi, 2003; Tesi et al., 2008; Tesi et al., 2007). Therefore, in our hypothesis, lignin concentration reflects

653   post-depositional degradation efficiency rather than original river input.

654   In this scenario, early diagenesis during burial is limited in the deep basin where anoxic sediments

655   hamper the complete OC breakdown including the terrestrial fraction. This would explain the relatively

656   high lignin content in the deepest station during S1 as well as the similarities between lignin content and

657   bulk OC (Fig. ~~7~~6 a, b, c and ~~11~~12). Taken together, our results indicate that terrestrial biomarkers in

658   sapropel beds do not necessarily reflect a primary signal (river input) but rather a secondary signal

659   (diagenesis) as observed for other "non-conservative" variables measured in sapropel bed~~s~~s such ~~as δ^{15}N,~~

660   pollen assemblages as well as other organic biomarkers (Cheddadi and Rossignol-Strick, 1995; Langgut et

661   al., 2011; Versteegh et al., 2010). Another recent example is the δ^{15}N whose depleted isotope composition

662   has been interpreted for a long time as a sign of enhanced primary productivity (Calvert et al., 1992).

663   Recent works showed that the lack of isotopic fractionation during early diagenesis is essentially the

664   reason why sapropel beds display depleted δ^{15}N signatures (Möbius et al., 2010; Sachs and Repeta, 1999).

665   Thus, as observed for the terrestrial biomarkers, the δ^{15}N signature in sapropel beds reflects a preservation

666   signal (diagenesis) rather than the original marine OC fingerprint.

667

668   Given the evident complications with the use of terrestrial biomarkers we have looked into the

669   literature (Combourieu-Nebout et al., 2013; Magny et al., 2012; Spötl et al., 2010) to find indications of

670   enhanced river discharge from the northern Mediterranean borderlands to justify the sapropel onset at

671   around 10 cal ky BP. The collective evidence based on speleothems, pollen data and debris flow fans and

672   lake levels suggests precipitation anomalies around 7.3 8.2-7.3 cal. ky BP (Spötl et al., 2010; Zanchetta et

673   al., 2007) over the northern Mediterranean Italian drainage basins regions (Alps and northern Apennine

674   chain)(i.e., Alps). (Magny et al., 2013)The wetter conditions during this period might have further

675   weakened the NADW during the sapropel deposition and stimulated the primary productivity. However,

676   other studies based on lake levels suggest conditions not particularly wet during the same period in

677   northern Italy (Magny et al., 2013). Despite the lack of agreement, (Spötl et al., 2010; Zanchetta et al.,

678   2007)it seems evident that this time interval (8.2-7.3 cal. ky BP) (Spötl et al., 2010; Zanchetta et al., 2007)

679   .is more which is more consistent with the second phase of sapropel S1 (S1b) rather than its the onset (ca.

680   10 cal ky BP). In conclusions, there is no evidence in the literature or in our river-proxy data suggesting

681   that S1 in the Adriatic was initiated by enhanced freshwater discharge from local rivers. By contrast, the

682   synchronous onset across the entire EMS suggests a wide-basin, physical-driven mechanism such as the

683   abrupt weakening of the LIW which hampered the dense water formation over the entire Eastern

684   Mediterranean Sea.

685

686

Conclusions

688   This study has redefined the conditions under which the Adriatic S1 formed. Our multifaceted

689   study based on integrated ecological, organic and inorganic parameters indicates that the weakening of the

690   NAdDW Northern Adriatic Deep Water exerted first-order control on the development of anoxic bottom

691   waters in the Adriatic as well as nearby deep basins such as the Ionian Sea. The emerging picture suggests

692   a chain of events in which the intensification of monsoon precipitation over North Africa followed by the

693   weakening of the LIW Levantine Intermediate Water ultimately suppressed the Northern Adriatic Deep

694   Water formation whichNAdDW leading to the S1 formation in the Adriatic and in those basins further

695   south under, consequently, hampered the the direct influence of the Eastern Mediterranean Deep

696 WaterEMDW~~Adriatic~~ ~~(e.g. Ionian basin,~~ developmentFig.11). As a result, the expression of the monsoon-

697 fuelled freshening was a synchronous stagnation ~~S1 formation~~ across the entire Eastern Mediterranean Sea

698 including the Adriatic. ~~Finally, our results rule out the increase of nutrient supply as the major driver for~~

699 ~~the S1 formation in Adriatic sediments.~~

700

701

702 **Acknowledgments**

710

711

712

713

714

715 **References**

716 Ariztegui, D., Asioli, A., Lowe, J.J., Trincardi, F., Vigliotti, L., Tamburini, F., Chondrogianni, C., Accorsi, C.A.,
717 Bandini Mazzanti, M., Mercuri, A.M., Van der Kaars, S., McKenzie, J.A., Oldfield, F., 2000. Palaeoclimate
718 and the formation of sapropel S1: inferences from Late Quaternary lacustrine and marine sequences in
719 the central Mediterranean region. Palaeogeography, Palaeoclimatology, Palaeoecology 158, 215-240.
720 Asioli, A., Trincardi, F., Lowe, J., Ariztegui, D., Langone, L., Oldfield, F., 2001. Sub-millennial scale climatic
721 oscillations in the central Adriatic during the Lateglacial: palaeoceanographic implications. Quaternary
722 Science Reviews 20, 1201-1221.

723 Asioli, A., Trincardi, F., Lowe, J., Oldfield, F., 1999. Short-term climate changes during the Last Glacial–
724 Holocene transition: comparison between Mediterranean records and the GRIP event stratigraphy.
725 Journal of Quaternary Science 14, 373-381.

726 Béthoux, J.-P., Pierre, C., 1999. Mediterranean functioning and sapropel formation: respective influences
727 of climate and hydrological changes in the Atlantic and the Mediterranean. Marine Geology 153, 29-39.

728 Bianchi, G., Hall, I.R., McCave, I., Joseph, L., 1999. Measurement of the sortable silt current speed proxy
729 using the Sedigraph 5100 and Coulter Multisizer IIe: Precision and accuracy. Sedimentology 46, 1001-
730 1014.

731 Blockley, S.P., Lowe, J.J., Walker, M.J., Asioli, A., Trincardi, F., Coope, G.R., Donahue, R.E., 2004. Bayesian
732 analysis of radiocarbon chronologies: examples from the European Late-glacial. Journal of Quaternary
733 Science 19, 159-175.

734 Bouloubassi, I., Rullkötter, J., Meyers, P.A., 1999. Origin and transformation of organic matter in
735 Pliocene–Pleistocene Mediterranean sapropels: organic geochemical evidence reviewed. Marine
736 Geology 153, 177-197.

737 Bröder, L., Tesi, T., Salvadó, J.A., Semiletov, I.P., Dudarev, O.V., Gustafsson, Ö., 2016. Fate of terrigenous
738 organic matter across the Laptev Sea from the mouth of the Lena River to the deep sea of the Arctic
739 interior. Biogeosciences 13, 5003-5019.

740 Calanchi, N., Dinelli, E., 2008. Tephrostratigraphy of the last 170 ka in sedimentary successions from the
741 Adriatic Sea. Journal of Volcanology and Geothermal Research 177, 81-95.

742 Calvert, S., Nielsen, B., Fontugne, M., 1992. Evidence from nitrogen isotope ratios for enhanced
743 productivity during formation of eastern Mediterranean sapropels.

744 Capotondi, L., Borsetti, A.M., Morigi, C., 1999. Foraminiferal ecozones, a high resolution proxy for the
745 late Quaternary biochronology in the central Mediterranean Sea. Marine Geology 153, 253-274.

746 Caron, B., Siani, G., Sulpizio, R., Zanchetta, G., Paterne, M., Santacroce, R., Tema, E., Zanella, E., 2012.
747 Late Pleistocene to Holocene tephrostratigraphic record from the Northern Ionian Sea. Marine Geology
748 311, 41-51.

749 Cheddadi, R., Rossignol-Strick, M., 1995. Improved preservation of organic matter and pollen in eastern
750 Mediterranean sapropels. Paleoceanography 10, 301-309.

751 Combourieu-Nebout, N., Peyron, O., Bout-Roumazeilles, V., Goring, S., Dormoy, I., Joannin, S., Sadori, L.,
752 Siani, G., Magny, M., 2013. Holocene vegetation and climate changes in the central Mediterranean
753 inferred from a high-resolution marine pollen record (Adriatic Sea). Climate of the Past 9, 2023-2042.

754 De Lange, G.J., Thomson, J., Reitz, A., Slomp, C.P., Principato, M.S., Erba, E., Corselli, C., 2008.
755 Synchronous basin-wide formation and redox-controlled preservation of a Mediterranean sapropel.
756 Nature Geoscience 1, 606-610.

757 Favaretto, S., Asioli, A., Miola, A., Piva, A., 2008. Preboreal climatic oscillations recorded by pollen and
758 foraminifera in the southern Adriatic Sea. Quaternary International 190, 89-102.

759 Filippidi, A., Triantaphyllou, M.V., De Lange, G.J., 2016. Eastern-Mediterranean ventilation variability
760 during sapropel S1 formation, evaluated at two sites influenced by deep-water formation from Adriatic
761 and Aegean Seas. Quaternary Science Reviews 144, 95-106.

762 Giunta, S., Negri, A., Morigi, C., Capotondi, L., Combourieu-Nebout, N., Emeis, K., Sangiorgi, F., Vigliotti,
763 L., 2003. Coccolithophorid ecostratigraphy and multi-proxy paleoceanographic reconstruction in the
764 Southern Adriatic Sea during the last deglacial time (Core AD91-17). Palaeogeography,
765 Palaeoclimatology, Palaeoecology 190, 39-59.

766 Gogou, A., Bouloubassi, I., Lykousis, V., Arnaboldi, M., Gaitani, P., Meyers, P.A., 2007. Organic
767 geochemical evidence of Late Glacial–Holocene climate instability in the North Aegean Sea.
768 Palaeogeography, Palaeoclimatology, Palaeoecology 256, 1-20.

769 Gordon, E.S., Goñi, M.A., 2003. Sources and distribution of terrigenous organic matter delivered by the
770 Atchafalaya River to sediments in the northern Gulf of Mexico. Geochimica et Cosmochimica Acta 67,
771 2359-2375.

772 Grimm, R., Maier-Reimer, E., Mikolajewicz, U., Schmiedl, G., Müller-Navarra, K., Adloff, F., Grant, K.M.,
773 Ziegler, M., Lourens, L.J., Emeis, K.-C., 2015. Late glacial initiation of Holocene eastern Mediterranean
774 sapropel formation. Nature communications 6.

775 Hennekam, R., Jilbert, T., Schnetger, B., Lange, G.J., 2014. Solar forcing of Nile discharge and sapropel S1
776 formation in the early to middle Holocene eastern Mediterranean. Paleoceanography 29, 343-356.

777 Hilgen, F., 1991. Astronomical calibration of Gauss to Matuyama sapropels in the Mediterranean and
778 implication for the geomagnetic polarity time scale. Earth and planetary science letters 104, 226-244.

779 Jorissen, F.J., 1988. Benthic foraminifera from the Adriatic Sea: principles of phenotypic variation.
780 Utrecht Micropaleontological Bulletins 37.

781 Jorissen, F.J., 1999. Benthic foraminiferal successions across Late Quaternary Mediterranean sapropels.
782 Marine Geology 153, 91-101.

783 Jorissen, F.J., Asioli, A., Borsetti, A., Capotondi, L., De Visser, J., Hilgen, F., Rohling, E., Van der Borg, K.,
784 Grazzini, C.V., Zachariasse, W., 1993. Late quaternary central Mediterranean biochronology. Marine
785 Micropaleontology 21, 169-189.

786 Klein, B., Roether, W., Civitarese, G., Gacic, M., Manca, B.B., d'Alcala, M.R., 2000. Is the Adriatic returning
787 to dominate the production of Eastern Mediterranean Deep Water. Geophys. Res. Lett 27, 3377-3380.

788 Kotthoff, U., Pross, J., Müller, U.C., Peyron, O., Schmiedl, G., Schulz, H., Bordon, A., 2008. Climate
789 dynamics in the borderlands of the Aegean Sea during formation of sapropel S1 deduced from a marine
790 pollen record. Quaternary Science Reviews 27, 832-845.

791 Langgut, D., Almogi-Labin, A., Bar-Matthews, M., Weinstein-Evron, M., 2011. Vegetation and climate
792 changes in the South Eastern Mediterranean during the Last Glacial-Interglacial cycle (86 ka): new marine
793 pollen record. Quaternary Science Reviews 30, 3960-3972.

794 Langone, L., Conese, I., Miserocchi, S., Boldrin, A., Bonaldo, D., Carniel, S., Chiggiato, J., Turchetto, M.,
795 Borghini, M., Tesi, T., 2015. Dynamics of particles along the western margin of the Southern Adriatic:
796 Processes involved in transferring particulate matter to the deep basin. Marine Geology.

797 Lowe, J.J., Blockley, S., Trincardi, F., Asioli, A., Cattaneo, A., Matthews, I.P., Pollard, M., Wulf, S., 2007.
798 Age modelling of late Quaternary marine sequences in the Adriatic: Towards improved precision and
799 accuracy using volcanic event stratigraphy. Continental Shelf Research 27, 560-582.

800 Magny, M., Combourieu-Nebout, N., De Beaulieu, J., Bout-Roumazeilles, V., Colombaroli, D., Desprat, S.,
801 Francke, A., Joannin, S., Peyron, O., Revel, M., 2013. North-south palaeohydrological contrasts in the
802 central Mediterranean during the Holocene: tentative synthesis and working hypotheses. Climate of the
803 Past Discussions 9, 1901-1967 (IF 1903,1509).

804 Magny, M., Joannin, S., Galop, D., Vannière, B., Haas, J.N., Bassetti, M., Bellintani, P., Scandolari, R.,
805 Desmet, M., 2012. Holocene palaeohydrological changes in the northern Mediterranean borderlands as
806 reflected by the lake-level record of Lake Ledro, northeastern Italy. Quaternary Research 77, 382-396.

807 Marchini, G., Zanchetta, G., Santacroce, R., Vigliotti, L., Capotondi, L., Sulpizio, R., 2014.
808 Tephrostratigraphy of marine core AD91-17 (Adriatic Sea) Revised. Alpine and Mediterranean
809 Quaternary 27, 77-84.

810 Marini, M., Maselli, V., Campanelli, A., Foglini, F., Grilli, F., 2015. Role of the Mid-Adriatic deep in dense
811 water interception and modification. Marine Geology.

812 Marino, G., Rohling, E.J., Sangiorgi, F., Hayes, A., Casford, J.L., Lotter, A.F., Kucera, M., Brinkhuis, H., 2009.
813 Early and middle Holocene in the Aegean Sea: interplay between high and low latitude climate
814 variability. Quaternary Science Reviews 28, 3246-3262.

815 McCave, I., Hall, I.R., 2006. Size sorting in marine muds: Processes, pitfalls, and prospects for
816 paleoflow-speed proxies. Geochemistry, Geophysics, Geosystems 7.

817   Mercone, D., Thomson, J., Abu-Zied, R., Croudace, I., Rohling, E., 2001. High-resolution geochemical and
818   micropalaeontological profiling of the most recent eastern Mediterranean sapropel. Marine Geology
819   177, 25-44.
820   Mercone, D., Thomson, J., Croudace, I., Siani, G., Paterne, M., Troelstra, S., 2000. Duration of S1, the
821   most recent sapropel in the eastern Mediterranean Sea, as indicated by accelerator mass spectrometry
822   radiocarbon and geochemical evidence. Paleoceanography 15, 336-347.
823   Millot, C., 1999. Circulation in the western Mediterranean Sea. Journal of Marine Systems 20, 423-442.
824   Minisini, D., Trincardi, F., Asioli, A., 2006. Evidence of slope instability in the Southwestern Adriatic
825   Margin. Natural Hazards and Earth System Science 6, 1-20.
826   Möbius, J., Lahajnar, N., Emeis, K.-C., 2010. Diagenetic control of nitrogen isotope ratios in Holocene
827   sapropels and recent sediments from the Eastern Mediterranean Sea. Biogeosciences 7, 3901-3914.
828   Narciso, Á., Flores, J.-A., Cachão, M., Piva, A., Asioli, A., Andersen, N., Schneider, R., 2012. Late Glacial–
829   Holocene transition in the southern Adriatic Sea: Coccolithophore and Foraminiferal evidence.
830   micropaleontology, 523-538.
831   Nieuwenhuize, J., Maas, Y.E.M., Middelburg, J.J., 1994. Rapid analysis of organic carbon and nitrogen in
832   particulate materials. Marine Chemistry 45, 217-224.
833   Nijenhuis, I., Schenau, S., Van der Weijden, C., Hilgen, F., Lourens, L., Zachariasse, W., 1996. On the origin
834   of upper Miocene sapropelites: a case study from the Faneromeni section, Crete (Greece).
835   Paleoceanography 11, 633-645.
836   Passier, H.F., Middelburg, J.J., de Lange, G.J., Böttcher, M.E., 1997. Pyrite contents, microtextures, and
837   sulfur isotopes in relation to formation of the youngest eastern Mediterranean sapropel. Geology 25,
838   519-522.
839   Piva, A., 2007. Stratigrafia ad alta risoluzione dei depositi Quaternari in Adriatico centrale e
840   meridionale:impatto di cambiamenti climatici a scala sub-Milankoviana sulla circolazione in
841   Mediterraneo, University of Bologna. Bologna, Bologna.
842   Piva, A., Asioli, A., Trincardi, F., Schneider, R.R., Vigliotti, L., 2008. Late-Holocene climate variability in the
843   Adriatic sea (Central Mediterranean). The Holocene 18, 153-167.
844   Ramsey, C.B., 1995. Radiocarbon calibration and analysis of stratigraphy; the OxCal program.
845   Radiocarbon 37, 425-430.
846   Ramsey, C.B., Lee, S., 2013. Recent and planned developments of the program OxCal. Radiocarbon 55,
847   720-730.
848   Reimer, P.J., Bard, E., Bayliss, A., Beck, J.W., Blackwell, P.G., Bronk Ramsey, C., Buck, C.E., Cheng, H.,
849   Edwards, R.L., Friedrich, M., 2013. IntCal13 and Marine13 radiocarbon age calibration curves 0-50,000
850   years cal BP.
851   Reitz, A., Thomson, J., de Lange, G.J., Hensen, C., 2006. Source and development of large manganese
852   enrichments above eastern Mediterranean sapropel S1. Paleoceanography 21.
853   Rogerson, M., Cacho, I., Jimenez-Espejo, F., Reguera, M.I., Sierro, F.J., Martinez-Ruiz, F., Frigola, J.,
854   Canals, M., 2008. A dynamic explanation for the origin of the western Mediterranean organic-rich layers.
855   Geochemistry, Geophysics, Geosystems 9, n/a-n/a.
856   Rohling, E., Bryden, H., 1994. Estimating past changes in the Eastern Mediterranean freshwater budget,
857   using reconstructions of sea level and hydrography. Proceedings of the Koninklijke Nederlandse
858   Akademie van Wetenschappen 97, 201-217.
859   Rohling, E., Jorissen, F., De Stigter, H., 1997. 200 year interruption of Holocene sapropel formation in the
860   Adriatic Sea. Journal of Micropalaeontology 16, 97-108.
861   Rohling, E., Marino, G., Grant, K., 2015. Mediterranean climate and oceanography, and the periodic
862   development of anoxic events (sapropels). Earth-Science Reviews 143, 62-97.
863   Rossignol-Strick, M., 1985. Mediterranean Quaternary sapropels, an immediate response of the African
864   monsoon to variation of insolation. Palaeogeography, palaeoclimatology, palaeoecology 49, 237-263.

865   Rossignol-Strick, M., Nesteroff, W., Olive, P., Vergnaud-Grazzini, C., 1982. After the deluge:
866   Mediterranean stagnation and sapropel formation.
867   Sachs, J.P., Repeta, D.J., 1999. Oligotrophy and nitrogen fixation during eastern Mediterranean sapropel
868   events. Science 286, 2485-2488.
869   Sangiorgi, F., Capotondi, L., Combourieu Nebout, N., Vigliotti, L., Brinkhuis, H., Giunta, S., Lotter, A.F.,
870   Morigi, C., Negri, A., Reichart, G.J., 2003. Holocene seasonal sea-surface temperature variations in the
871   southern Adriatic Sea inferred from a multiproxy approach. Journal of Quaternary Science 18, 723-732.
872   Santacroce, R., Cioni, R., Marianelli, P., Sbrana, A., Sulpizio, R., Zanchetta, G., Donahue, D.J., Joron, J.L.,
873   2008. Age and whole rock–glass compositions of proximal pyroclastics from the major explosive
874   eruptions of Somma-Vesuvius: a review as a tool for distal tephrostratigraphy. Journal of Volcanology
875   and Geothermal Research 177, 1-18.
876   Santvoort, P., Lange, G., Langereis, C., Dekkers, M., Paterne, M., 1997. Geochemical and paleomagnetic
877   evidence for the occurrence of "missing" sapropels in eastern Mediterranean sediments.
878   Paleoceanography 12, 773-786.
879   Schmiedl, G., Kuhnt, T., Ehrmann, W., Emeis, K.-C., Hamann, Y., Kotthoff, U., Dulski, P., Pross, J., 2010.
880   Climatic forcing of eastern Mediterranean deep-water formation and benthic ecosystems during the past
881   22 000 years. Quaternary Science Reviews 29, 3006-3020.
882   Schmiedl, G., Mitschele, A., Beck, S., Emeis, K.-C., Hemleben, C., Schulz, H., Sperling, M., Weldeab, S.,
883   2003. Benthic foraminiferal record of ecosystem variability in the eastern Mediterranean Sea during
884   times of sapropel S 5 and S 6 deposition. Palaeogeography, Palaeoclimatology, Palaeoecology 190, 139-
885   164.
886   Siani, G., Magny, M., Paterne, M., Debret, M., Fontugne, M., 2013. Paleohydrology reconstruction and
887   Holocene climate variability in the South Adriatic Sea. Climate of the Past 9, 499-515.
888   Siani, G., Paterne, M., Arnold, M., Bard, E., Métivier, B., Tisnerat, N., Bassinot, F., 2000. Radiocarbon
889   reservoir ages in the Mediterranean Sea and Black Sea. Radiocarbon 42, 271-280.
890   Siani, G., Paterne, M., Colin, C., 2010. Late glacial to Holocene planktic foraminifera bioevents and
891   climatic record in the South Adriatic Sea. Journal of Quaternary Science 25, 808-821.
892   Spagnoli, F., Dell'Anno, A., De Marco, A., Dinelli, E., Fabiano, M., Gadaleta, M.V., Ianni, C., Loiacono, F.,
893   Manini, E., Marini, M., 2010. Biogeochemistry, grain size and mineralogy of the central and southern
894   Adriatic Sea sediments: a review. Chemistry and Ecology 26, 19-44.
895   Spötl, C., Nicolussi, K., Patzelt, G., Boch, R., 2010. Humid climate during deposition of sapropel 1 in the
896   Mediterranean Sea: Assessing the influence on the Alps. Global and Planetary Change 71, 242-248.
897   Tachikawa, K., Vidal, L., Cornuault, M., Garcia, M., Pothin, A., Sonzogni, C., Bard, E., Menot, G., Revel, M.,
898   2015. Eastern Mediterranean Sea circulation inferred from the conditions of S1 sapropel deposition.
899   Clim. Past 11, 855-867.
900   Tesi, T., Langone, L., Goni, M., Turchetto, M., Miserocchi, S., Boldrin, A., 2008. Source and composition of
901   organic matter in the Bari canyon (Italy): dense water cascading versus particulate export from the upper
902   ocean. Deep Sea Research Part I: Oceanographic Research Papers 55, 813-831.
903   Tesi, T., Miserocchi, S., Goni, M.e.a., Langone, L., Boldrin, A., Turchetto, M., 2007. Organic matter origin
904   and distribution in suspended particulate materials and surficial sediments from the western Adriatic Sea
905   (Italy). Estuarine, Coastal and Shelf Science 73, 431-446.
906   Tesi, T., Semiletov, I., Hugelius, G., Dudarev, O., Kuhry, P., Gustafsson, Ö., 2014. Composition and fate of
907   terrigenous organic matter along the Arctic land–ocean continuum in East Siberia: Insights from
908   biomarkers and carbon isotopes. Geochimica et Cosmochimica Acta 133, 235-256.
909   Toucanne, S., Minto'o, C.M.A., Fontanier, C., Bassetti, M.-A., Jorry, S.J., Jouet, G., 2015. Tracking rainfall
910   in the northern Mediterranean borderlands during sapropel deposition. Quaternary Science Reviews
911   129, 178-195.

912 Trincardi, F., Cattaneo, A., Asioli, A., Correggiari, A., Langone, L., 1996. Stratigraphy of the late-
913 Quaternary deposits in the central Adriatic basin and the record of short-term climatic events.
914 MEMORIE-ISTITUTO ITALIANO DI IDROBIOLOGIA 55, 39-70.
915 Trincardi, F., Verdicchio, G., Miserocchi, S., 2007. Seafloor evidence for the interaction between
916 cascading and along-slope bottom water masses. Journal of Geophysical Research: Earth Surface 112.
917 Turchetto, M., Boldrin, A., Langone, L., Miserocchi, S., Tesi, T., Foglini, F., 2007. Particle transport in the
918 Bari canyon (southern Adriatic Sea). Marine Geology 246, 231-247.
919 Van Straaten, L., 1970. Holocene and late-Pleistocene sedimentation in the Adriatic Sea. Geologische
920 Rundschau 60, 106-131.
921 Versteegh, G.J.M., Zonneveld, K.A.F., de Lange, G.J., 2010. Selective aerobic and anaerobic degradation
922 of lipids and palynomorphs in the Eastern Mediterranean since the onset of sapropel S1 deposition.
923 Marine Geology 278, 177-192.
924 Vigliotti, L., Asioli, A., Bergami, C., Capotondi, L., Piva, A., 2011. Magnetic properties of the youngest
925 sapropel S1 in the Ionian and Adriatic Sea: inference for the timing and mechanism of sapropel
926 formation. Italian journal of geosciences 130, 106-118.
927 Vigliotti, L., Verosub, K., Cattaneo, A., Trincardi, F., Asioli, A., Piva, A., 2008. Palaeomagnetic and rock
928 magnetic analysis of Holocene deposits from the Adriatic Sea: detecting and dating short-term
929 fluctuations in sediment supply. The Holocene 18, 141-152.
930 Vilibić, I., Orlić, M., 2002. Adriatic water masses, their rates of formation and transport through the
931 Otranto Strait. Deep Sea Research Part I: Oceanographic Research Papers 49, 1321-1340.
932 Vilibić, I., Supić, N., 2005. Dense water generation on a shelf: the case of the Adriatic Sea. Ocean
933 Dynamics 55, 403-415.
934 Weldeab, S., Menke, V., Schmiedl, G., 2014. The pace of East African monsoon evolution during the
935 Holocene. Geophysical Research Letters 41, 1724-1732.
936 Zanchetta, G., Drysdale, R.N., Hellstrom, J.C., Fallick, A.E., Isola, I., Gagan, M.K., Pareschi, M.T., 2007.
937 Enhanced rainfall in the Western Mediterranean during deposition of sapropel S1: stalagmite evidence
938 from Corchia cave (Central Italy). Quaternary Science Reviews 26, 279-286.

939

940

941

942

943

944

945

946

947

948

949

951

952

953

954

955

Figure 1. Map of the study area in the Adriatic Sea. Coring sites are displayed as filled dots and labelled AMC99-1 (260 m water depth), SA03-1 (567 m water depth), INVAS12-10 (570 m water depth) and ST04-1 (1085 m water depth) respectively. Arrows show the main water masses which include the Levantine Intermediate Water (LIW, red, main path, and dashed red, northward intrusion with large inter-decadal variability), North ~~and South~~ Adriatic Deep Water (NAdDW ~~and SAdDW,~~ blue) and the Eastern Mediterranean Deep Water (EMDW, green). Dashed line roughly displays the position of the shoreline at the S1 onset. ~~The black line represents the location of the depth profile (Fig. 2a).~~ The upper right inset shows the main path of the LIW in the eastern and central Mediterranean Sea and the Nile runoff input

35

964

965

966

967

968

969

970

971

972

973

974

975

976

977

978

Figure 2. Chirp profiles of the coring sites along the shelf-basin continuum. (a) The depth profile graph displays the general location of the sediment cores in respect to the dominant water masses (NAdDW and LIW). Seismic profiles through the three coring sites: (b) shelf-adjacent (mid-Adriatic depression, AMC99-1), (c) slope (sediment wave field, SA03-1 and INVAS12-10) and (d) deep basin (ST04-1).

983

984

985

986

987

988

989

990

991

992

993

994

995

996

997

998

999

1000

1001

1002

1003

1004

1005

1006

1007

1008

1009   **Figure 3.** Sediment cores from the Adriatic Sea (Fig. 1 and 2). Lithology, photo, false colours and XRAY

1010   of AMC99-1 (a), photo non available);. INVAS12-10 (b); and ST04-1 (c).

1011

1012

1013

1014

1015

1016

1017

1018

1019

1020

1021

1022

1023

1024

1025

1026

1027

1028

1029

1030

Figure 4. Down-core biostratigraphy of ST04-1, SA03-1 and AMC99-1. Four bioevents were used for the age-depth model: I (top YD, blue line), II (older peak *G. inflata*, light green), III (younger peak *G. inflata*, dark green), IV (last occurrence *G. inflata*, red line). For further details on the bioevents see Table 1 and method section. The figure shows also the correlation between twins core Core SA03-1 and INVAS12-10. collected in the sediment wave field. Cross-correlation between twin cores relays on bioevents and tephra (magnetic susceptibility anomalies). Events in chronological order include: top of the Younger Dryas, two *Globorotalia inflata* peaks (during the Pre Boreal), peak of *Cassidulinoides bradyi*, a large magnetic susceptibility peak marking a tephra layer, two *G. inflata* peaks (during S1 break and S1b, respectively) and the last Occurrence of *G. inflata*

1046

1047

1048

1049

1050

1051

1052

1053

1054

1055

1056

1057

1058

1059

1060

1061   **Figure 5.** Bayesian age-depth model of Adriatic records (median, 1σ and 2σ). Filled symbols (circles,

1062   squares and diamonds) show the radiocarbon dates used for the Bayesian model. Dark gray areas display

1063   distinct bioevents used to increase the model resolution and synchronize the records. The model shows

1064   good agreement between bioevents and the new radiocarbon dates of monospecific tests. For further

1065   details about the age-depth model see the method section. The paleoceanographic (and stratigraphic)

1066   events were identified independently in each core; therefore, all dates in each core are consistent and

1067   independent as no age is exported from one core to another.

1068

Figure 76. Sapropel S1 along the Adriatic shelf-basin continuum and external environmental forcings.
Organic carbon (OC) content of (a) ST04-1, (b) INVAS12-10 and (c) AMC99-1. Note the different scale
of y-axes. Bottom current proxesproxies: abundance of reworked inner-shelf foraminifera (d) and sortable

1108 silt (e) over the slope (SA03-1). (f) Nile runoff proxy: Ba/Ca of *Globigerinoides ruber* (Weldeab et al.,

1109 2014). Light and dark grey areas denote pre-sapropel sediments, the S1 boundaries and the sapropel S1

1110 break based on the OC content of ST04-1.

1111

1112

1113

1114

1115

1116

1117

1118

1119

1120

1121

1122

1123

1124

1125

1126

1127

1128

1129 **Figure 87.** Seafloor oxygen content and reducing conditions during the sapropel S1 deposition in Adriatic

1130 sediment along the shelf-basin continuum. Foraminifera-based oxygen index (OI, (Schmiedl et al., 2010)

1131   of (a) ST04-1, (b) SA03-01 and AMC99-1). Value of 1 refers to fully oxygenated conditions while 0

1132   represents azoic environment, respectively. Note, OI of AMC99-1 is based on intermediate infaunal

1133   foraminifera. Authigenic vanadium enrichment (V/Ti) of (ad) ST04-1, (be) SA03-01 and (f) AMC99-1.

1134   Light and dark grey areas show pre-sapropel sediments, the S1 boundaries and interruption based on the

1135   OC content of ST04-1 (see Fig. 16).

1136

1137

1138

1139

1140

1141

1142

1143

1144

1145

1146

1147

1148

1149

1150

1151

1152

1153

Figure 9<u>8</u>. Pre-sapropel and sapropel S1 onset in the Adriatic basin (ST04-1, 1085 m). (a) Organic carbon (OC) and oxygen index. (b) Abundance of deep and intermediate infaunal foraminifera and authigenic vanadium enrichment (V/TiO_2). Light grey area shows the azoic environment.

Figure ~~10~~9. Distribution of manganese and sulfur during the S1 deposition in Adriatic sediments along the shelf-basin continuum. Authigenic manganese enrichment of (a) ST04-1, (b) INVAS12-10 and (c) AMC99-1. Authigenic sulfur enrichment of (d) ST04-1, (e) INVAS12-10 and (f) AMC99-1. Light and dark grey areas show pre-sapropel sediments, S1 boundaries and interruption based on the OC content of ST04-1 (see Fig. 6). ~~. Light and dark grey areas show the S1 boundaries and interruption based on the OC content (see Fig. 1).~~ Note the different scale of y-axes.

Figure 10. Benthic ecosystem changes over water depth during the sapropel S1 deposition according to the foraminifera-based oxygen index. Changes were defined using the oxygen index threshold according to Schmiedl et al. (2010). Values less than 0.5 indicate the collapse of the benthic ecosystem while values more than 0.5 indicate the recovery of the benthic ecosystem. Solid line and grey area show mean and standard deviation of the S1 onset, respectively. Dashed line (interpolation water depth *vs* time) exhibits the progressive ventilation with increasing water depth over time. Aegean and Levantine data from Schmiedl et al. (2010).

Figure ~~6~~11. Comparison between sediment cores collected in the southern Adriatic basin. ST04-1 (this study), IN68-9 (Rohling et al., 1997), MD90-197 (Mercone et al., 2001; Siani et al., 2010) and AD90-17 (Capotondi et al., 1999). A) Location of the sediment cores. B) Core description, biostratrigraphy and bioevents (coloured lines). C) Core description and V/Al ratio (MD90-197 vs ST04-1). Radiocarbon dates shown in the figure refer to uncalibrated data (^{14}C yBP) for a direct comparison.

1202

1203

1204

1205

1206

1207

1208

1209

1210

1211

1212

1213

1214

1215

1216 **Figure 12~~1~~.** Terrigenous organic carbon concentration during the sapropel S1 deposition in Adriatic

1217 sediments along the shelf-basin continuum. Lignin concentration of (a) ST04-1, (b) INVAS12-10 and (c)

1218 AMC99-1. ~~Light and dark grey areas show the S1 boundaries and interruption based on the OC content~~

1219 ~~(see Fig. 1).~~ Light and dark grey areas show pre-sapropel sediments, S1 boundaries and interruption based

1220 on the OC content of ST04-1 (see Fig. 6).~~.~~ Note the different scale of y-axes.

1221

1222

1223

1224

1225

1226

1227

1228

1229

1230

1231
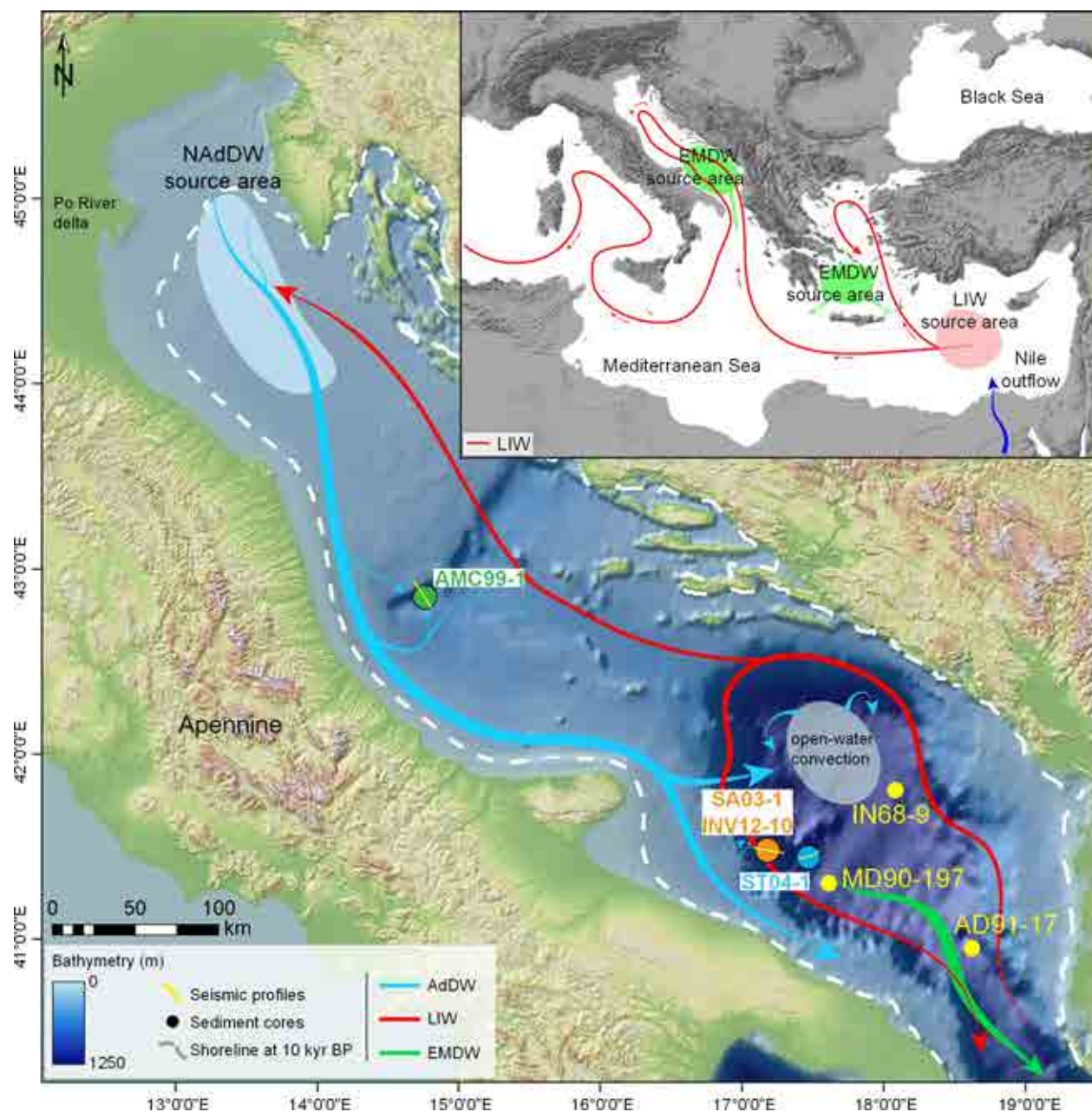
1232

1233

1234

1235

1236

1237

1238 **Figure 12.** ~~Cartoon of the thermohaline circulation: (a) modern conditions and (b) during the freshening~~

1239 ~~of the Eastern Mediterranean Sea via the Nile (b). As the precipitation increases over North Africa, the~~

1240 ~~Levantine Intermediate Waters (LIW) progressively decreases. This is turn hampers the preconditioning~~

1241 ~~North Adriatic Deep Water with cascade effects on the Eastern Mediterranean Deep Water formation. The~~

1242 ~~expression of the monsoon-fuelled freshening was a synchronous S1 formation across the Eastern~~

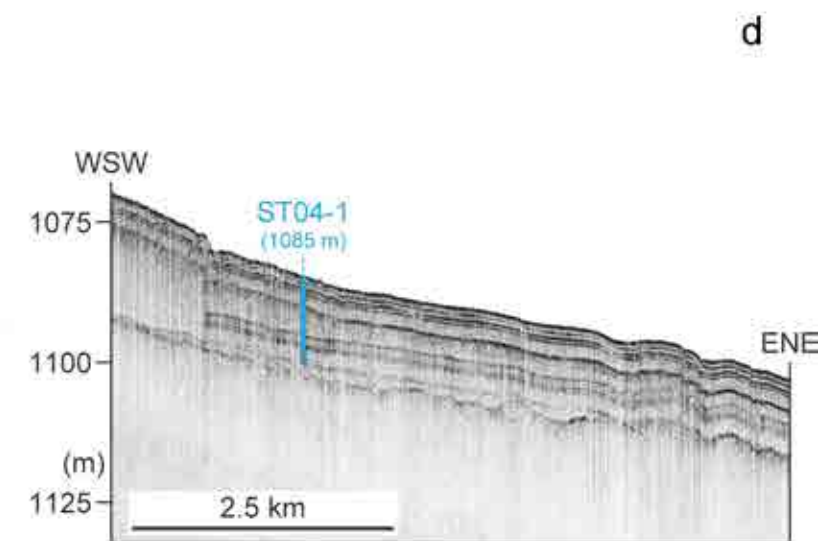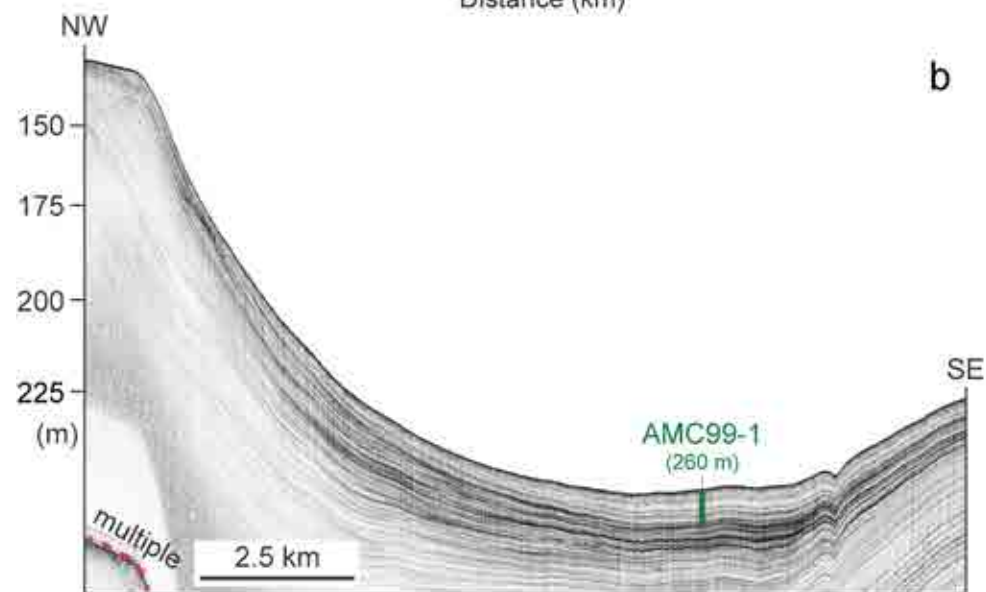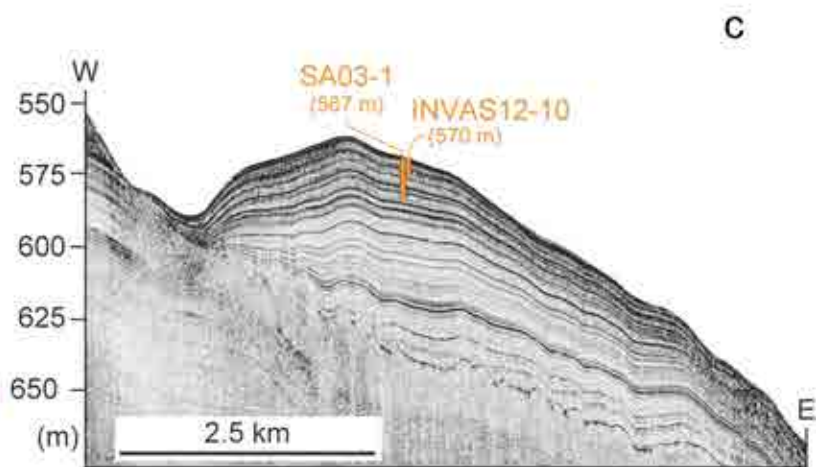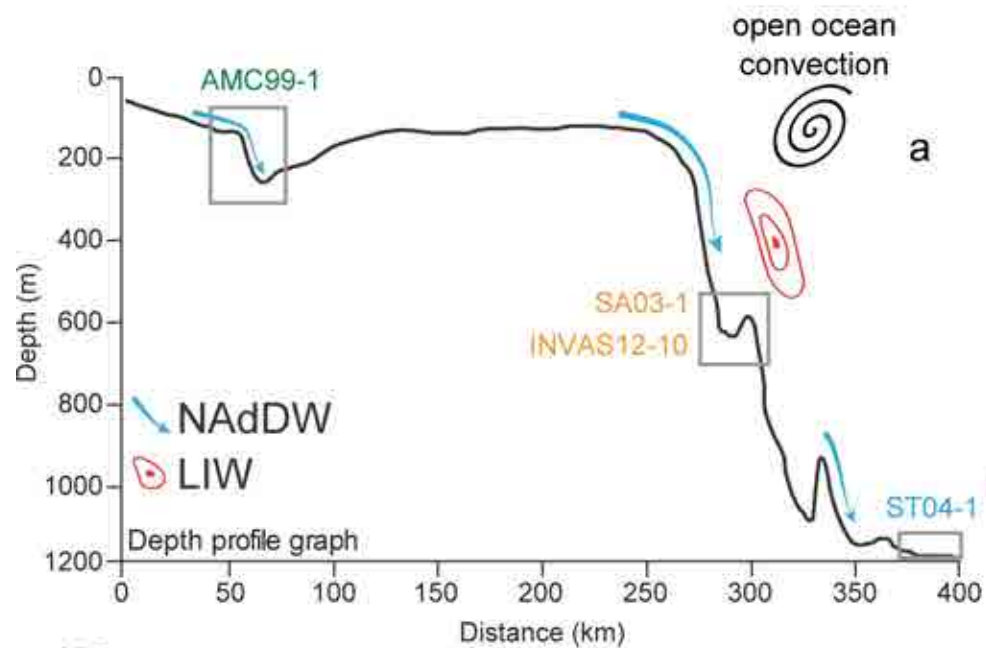1243 ~~Mediterranean Sea including the Adriatic.~~

Table S1. Dated levels used for the Bayesian age-depth model of core AMC991, INVAS12-10, ST04-1. The table contains a new radiocarbon date of core IN68-9 as well.

Lab. #	Core depth (cm)	Sample type	^{14}C age (yBP)	Modelled age (median, cal yBP)	-2δ	+2δ	Reference
AMC99-1 (260 m w.d.)							
Poz-16133	21-22	*Cibicidoides pachyderma*	1405 ± 30	629	720	530	Piva et al. (2008)
Poz-16134	117-118	*Cibicidoides pachyderma*	2880 ± 40	2208	2331	2073	Piva et al. (2008)
Poz-16135	222-223	*Cibicidoides pachyderma*	4200 ± 40	3889	4065	3724	Piva et al. (2008)
Poz-16137	258-259	mixed planktic	4570 ± 50	4630	4798	4464	Piva et al. (2008)
CAMS-33373	323-324	mixed planktic	5880 ± 60	6104	6265	5944	Bioevent IV, LO *G. inflata* (core RF93-30); (Trincardi et al., 1996)
OS-104703	374-375.5	*Globigerinoides ruber*	6720 ± 50	7046	7201	6906	this study
OS-104710	416-417	*Globigerinoides ruber*	7320 ± 60	7668	7805	7553	this study
OS-104283	470-471.5	*Globigerinoides ruber*	8230 ± 45	8565	8721	8420	this study
OS-104466	535-536	*Globigerinoides ruber*	9090 ± 35	9683	9856	9533	this study
Poz-16142	550-551	mixed planktic	9360 ± 50	10049	10184	9886	Bioevent III, Younger peak *G. inflata* (core SA03-1); (Favaretto et al., 2008)
Poz-16144	570-571	mixed planktic	9860 ± 60	10565	10727	10392	Bioevent II, Older peak *G. inflata* (core SA03-1); (Favaretto et al., 2008)
CAMS-16305	610-611	mixed planktic	10450 ± 90	11301	11623	11112	Bioevent I, Top YD (core CM92-43); (Asioli et al., 2001)
INVAS12-10 (570 m w.d.)							
CAMS-33373	275-276	mixed planktic	5880 ± 60	6116	6277	5937	Bioevent IV, LO *G. inflata* (core RF93-30); (Trincardi et al., 1996)
OS-104282	305-306	*Globigerinoides ruber*	6450 ± 35	6833	7115	6647	this study
OS-104380	319-320	*Globigerinoides ruber*	7340 ± 30	7648	7760	7558	this study
OS-108068	327-328	*Globigerinoides ruber*	7530 ± 60	7864	7986	7725	this study
OS-104381	347-348	*Globigerinoides ruber*	8240 ± 35	8565	8721	8421	this study

Lab code	Depth (cm)	Species	^{14}C age				Reference
OS-104382	375-376	*Globigerinoides ruber*	9140 ± 35	9596	9982	9151	this study
Poz-16142	389-390	mixed planktic	9360 ± 50	10100	10232	9885	Bioevent III, Younger peak *G. inflata* (core SA03-1); (Favaretto et al., 2008)
Poz-16144	395-396	mixed planktic	9860 ± 60	10577	10768	10373	Bioevent II, Older peak *G. inflata* (core SA03-1); (Favaretto et al., 2008)
CAMS-16305	413-414	mixed planktic	10450 ± 90	11301	11682	11088	Bioevent I, Top YD (core CM92-43); (Asioli et al., 2001)

ST04-1 (1085 m w.d.)

Lab code	Depth (cm)	Species	^{14}C age				Reference
CAMS-33373	80-81	mixed planktic	5880 ± 60	6103	6275	5925	Bioevent IV, LO *G. inflata* (core RF93-30); (Trincardi et al., 1996)
OS-104464	102-103	*Globigerinoides ruber*	6510 ± 30	6878	7011	6735	this study
OS-104378	113-114	*Globigerinoides ruber*	7160 ± 30	7521	7607	7425	this study
OS-104465	120-121	*Globigerinoides ruber*	7800 ± 35	8110	8254	7985	this study
OS-104281	139-140	*Globigerinoides ruber*	9040 ± 40	9562	9701	9455	this study
OS-107637	142-143	*Globigerinoides ruber*	9180 ± 40	9755	9916	9580	this study
Poz-16142	145-146	mixed planktic	9360 ± 50	10009	10181	9826	Bioevent III, Younger peak *G. inflata* (core SA03-1); (Favaretto et al., 2008)
Poz-16144	153-154	mixed planktic	9860 ± 60	10669	10842	10505	Bioevent II, Older peak *G. inflata* (core SA03-1); (Favaretto et al., 2008)
OS-104379	154-155	*Globorotalia inflata*	10050 ± 45	10761	10949	10624	this study
CAMS-16305	169-170	mixed planktic	10450 ± 90	11442	11790	11165	Bioevent I, Top YD (core CM92-43); (Asioli et al., 2001)

IN68-9 (1234 m w.d.)

Lab code	Depth (cm)	Species	^{14}C age				Reference
OS-127850	137-138	*Globigerinoides ruber*	9030 ± 30				Not calibrated for direct comparison with previous studies Rohling et al. (1997)

* For further details about biostratigraphy and bioevents see the method section in the main text
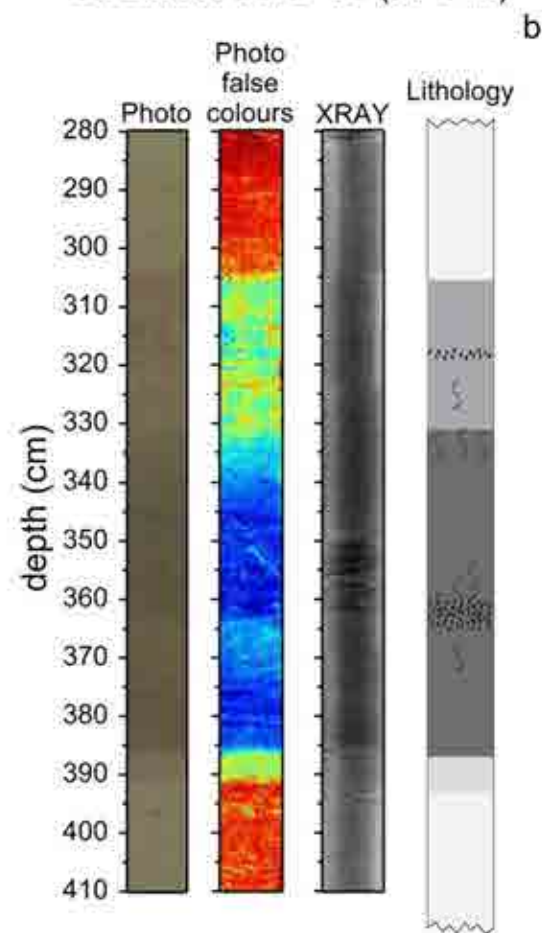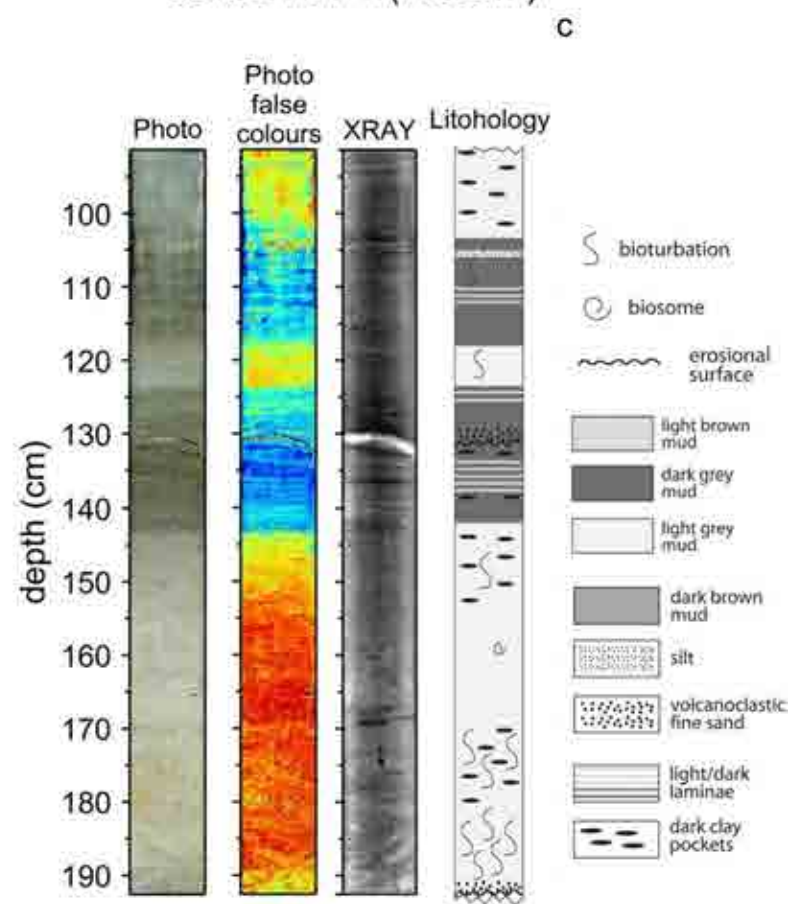
1244

a — Depth profile graph

AMC99-1

open ocean convection

SA03-1
INVAS12-10

NAdDW

LIW

ST04-1

b

NW

SE

AMC99-1
(260 m)

multiple

2.5 km

c

W

SA03-1
(567 m)

INVAS12-10
(570 m)

E

2.5 km

d

WSW

ST04-1
(1085 m)

ENE

2.5 km

core AMC99-1 (260 m)   a

core INVAS12-10 (570 m)   b

core ST04-1 (1085 m)   c

Lithology   XRAY

Photo   Photo false colours   XRAY   Lithology

Photo   Photo false colours   XRAY   Litohology

Legend:
- bioturbation
- biosome
- erosional surface
- light brown mud
- dark grey mud
- light grey mud
- dark brown mud
- silt
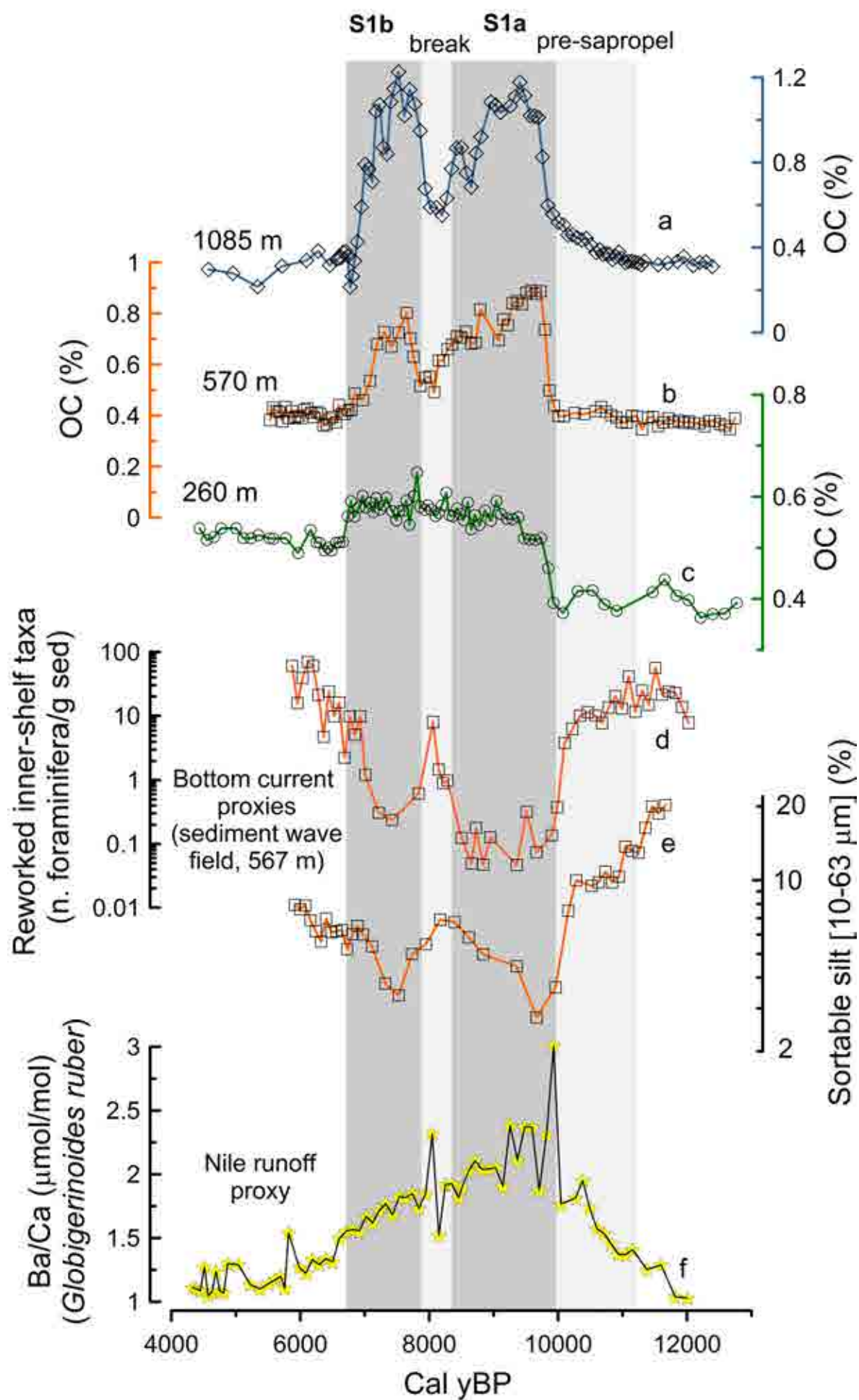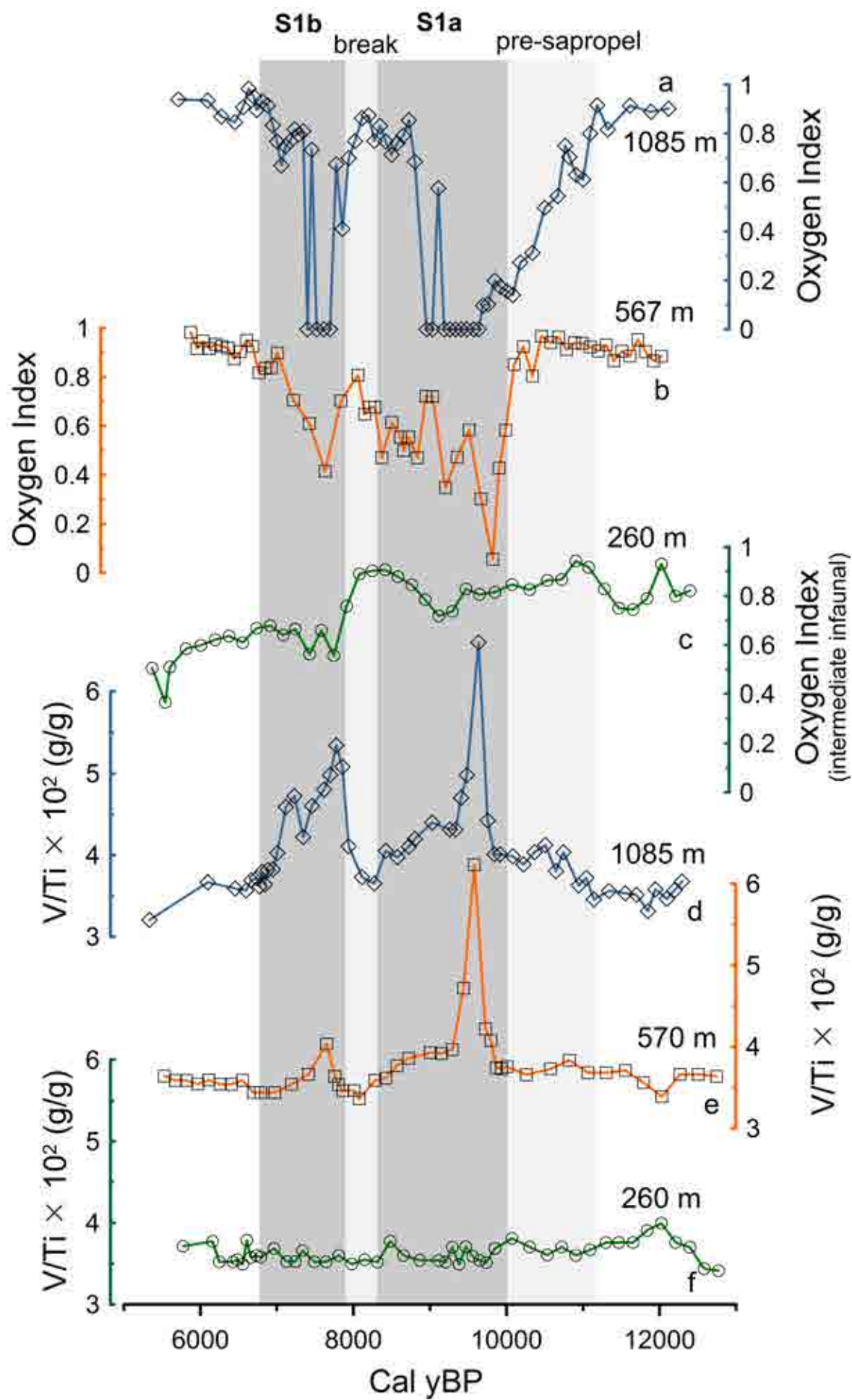- volcanoclastic fine sand
- light/dark laminae
- dark clay pockets

Core ST04-1 (w.d. 1085 m) Core SA03-1 (w.d. 567 m) Core AMC99-1 (w.d. 260 m)

K(10⁻⁶SI)
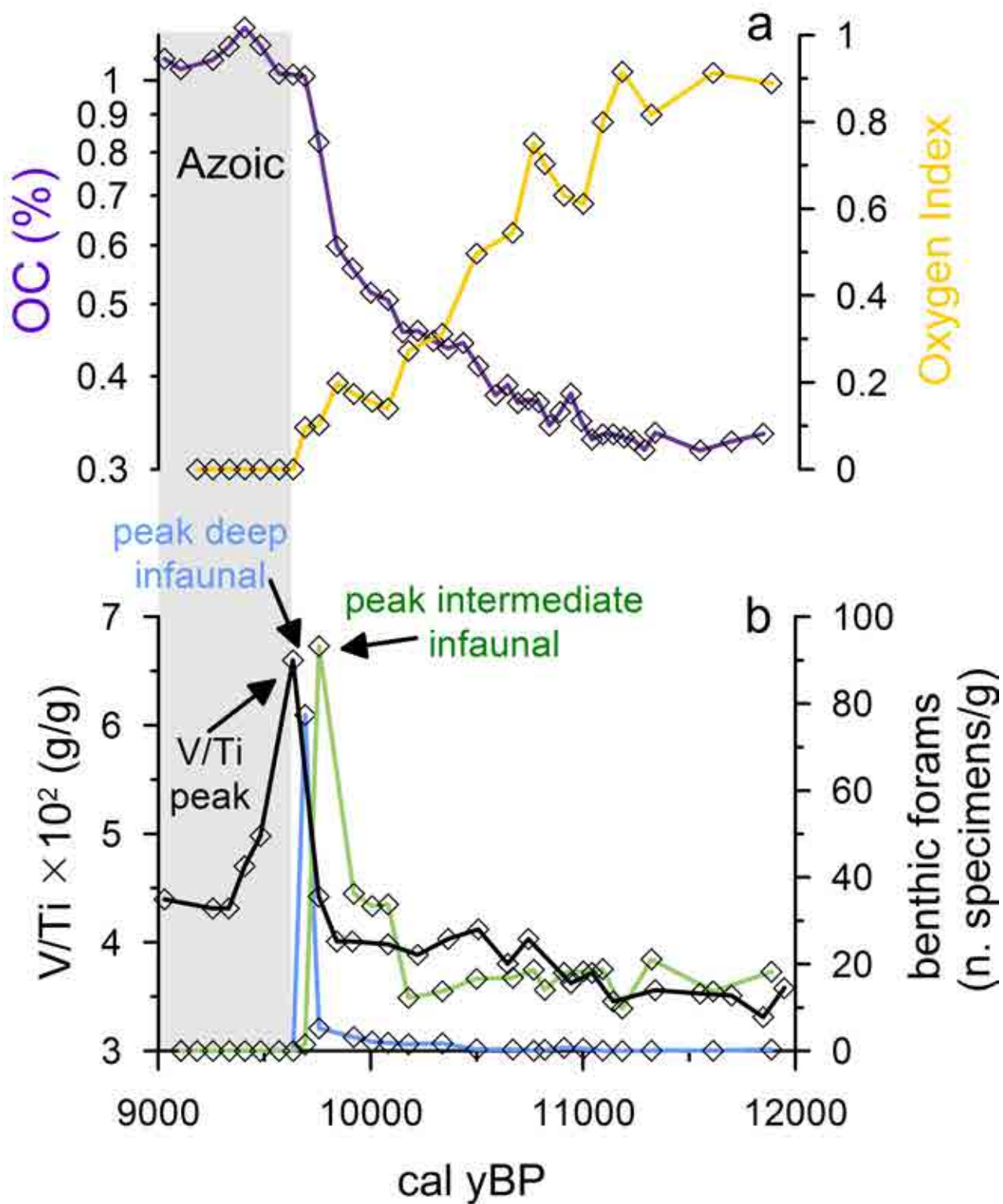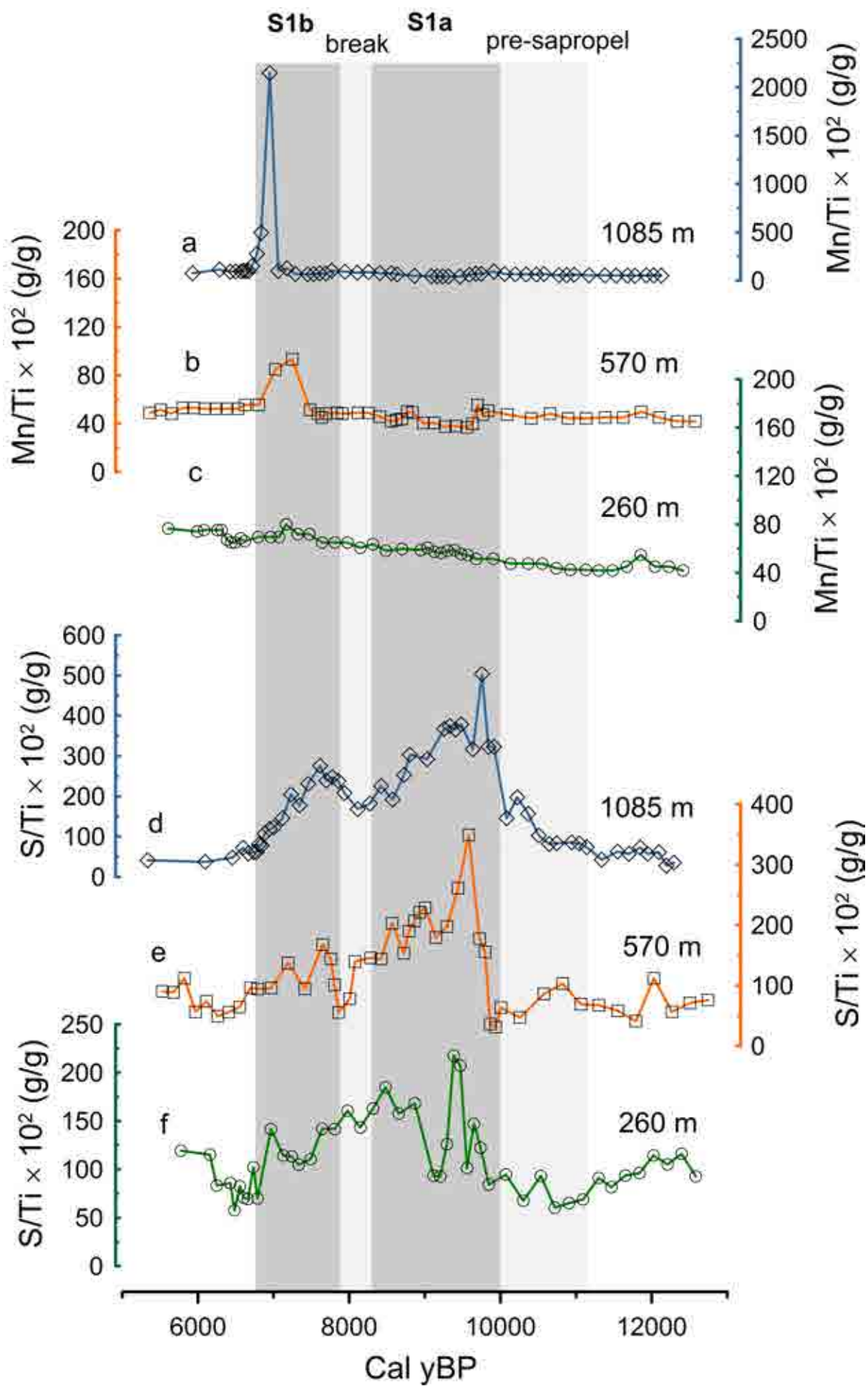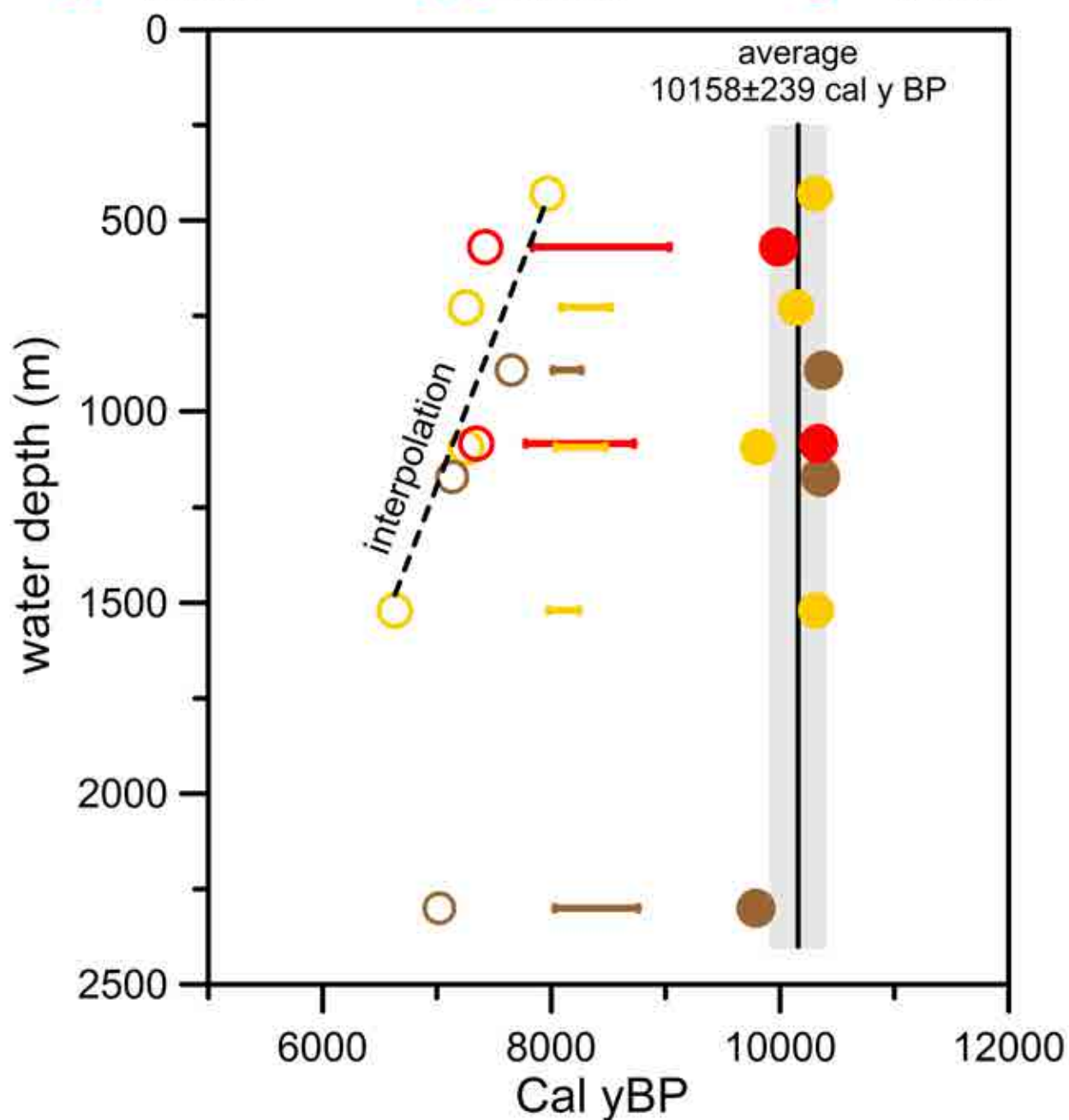0 200 400

G. ruber
0 10 20 30 40%

cm
70
80
90
100
110 S1b
120
130 S1a
140
150
160
170
180
190
0 10 20 30 40%
G. inflata

cm
200
300
400
500
600
0 10 20 30 40%
G. inflata

G. ruber
0 10 20 30 40%

0 20 40 60 80 100%
C. bradyi

Core INVAS12-10
(w.d. 570m)

K(10⁶SI)
0 100 200 300

cm
250
300
350
400
450
lithology

G. inflata re-entry
after S1b
G. inflata peak in
S1 interruption
volcanoclastic layer
peak C. bradyi

cm
250
300
350
400
450
500
550
600
650
700

G. ruber
0 10 20 30 40%

Bioevent IV
LO G. inflata

Bioevent III
Younger Peak
G. inflata

Bioevent II
older peak G. inflata

Bioevent I
top YD

GS-1
(Younger Dryas)

0 10 20 30 40%
G. inflata

S1b   break   S1a   pre-sapropel

1085 m

a

570 m

b

260 m

c

Bottom current proxies (sediment wave field, 567 m)

d

e

Nile runoff proxy

f

S1b · break · S1a · pre-sapropel

core ST04-1 (1085 m)

S1b   S1a
break   pre-sapropel

core AD91-17 (w.d. 844 m)
(after Capotondi et al., 1999;
Sangiorgi et al., 2003; Marchini et al., 2014)

core MD90-197 (w.d. 1010 m)
(after Siani et al., 2010)

core IN68-9 (w.d. 1234m)
after Rohling et al., 1997 and Calanchi et al., 2008

core ST04-1 (w.d. 1085m)

A

core MD90-197 (w.d. 1010 m)
(after Mercone et al., 2000, 2001;
Siani et al., 2004; Siani et al., 2010)

core ST04-1 (w.d. 1085m)

B

dark units (= Sapropel1) thickness
according to Mercone et al. (2001)

* monospecific samples

— Bioevent IV LO G. inflata
— G. rubescens peak
— G. ruber peak
— Bioevent III Younger peak G. inflata
— Bioevent II Older peak G. inflata
— Bioevent I TopYD

Tephra layers

AT   Astroni
AMS   Agnano Monte Spina
E1   Gabellotto-Fiumebianco
Mer   Mercato
Pal1   Capo Palinuro
C1   Agnano Pomici Principali

turbidite

In this section, we revisit the age-depth model originally presented by Rohling et al. (1997) using Oxcal. The new model allows for random fluctuations in sediment deposition (P_sequence) and benefits of a new radiocarbon date (monospecific planktonic test, *G. ruber*, reference OS-127850) (Table S1). In addition to the radiocarbon tests, the model relays on well-characterized, radiocarbon dated bioevents (I,II, III, IV) as specified in the main text and Table S1. Our overarching goal is to understand whether the offset (ca. 1ky) between our results and Rohling et al. (1997) is a consequence of the age-depth model constrain. The Oxcal script used to generate the model is reported below. Particular attention was given to the agreement index which measures the coherence between the model (prior) and the observational data (likelihood).

Radiocarbon test UTC-501 (Table 1; Fig. S1,S2,S3) turned out having a low agreement index (ca. 4%) (Fig. S3) and thus considered as an outlier. Altogether, our analysis revealed that the offset derives from this radiocarbon value being relatively young.

Table S1. Radiocarbon dates of core IN68-9

Lab. #	depth (cm)	Sample	^{14}C age (yr BP)	Source
UTC-500	11.5	benthic forams	3160 ± 120	Rohling et al. (1997)
CAMS-33373	43	mixed planktic	5880 ± 60	Bioevent IV, LO G. inflata (core RF93-30); Trincardi et al. (1996)
UTC-1607	54.5	mixed planktic	6390 ± 60	Rohling et al. (1997)
OS-127850	137.5	*Globigerinoides ruber*	9030 ± 30	this study
Poz-16142	143	mixed planktic	9360 ± 50	Bioevent III, Younger peak G. inflata (core SA03-1); Favaretto et al. (2008)
Poz-16144	155	mixed planktic	9860 ± 60	Bioevent II, Older peak G. inflata (core SA03-1); Favaretto et al. (2008)
UTC-501	156.5	benthic forams	9280 ± 180	Rohling et al. (1997)
CAMS-16305	162.5	mixed planktic	10450 ± 90	Bioevent I, Top YD (core CM92-43); Asioli et al. (2001)
UTC-502	241.5	mixed planktic	13100 ± 200	Rohling et al. (1997)

Oxcal script

```
Options()
 {
  BCAD=FALSE;
 };
 Plot()
 {
  Curve("Marine13","Marine13.14c");
  Delta_R("DeltaR based on Calib", 136, 41);


P_Sequence("variable", 1,1,U(-2,2))


   {

Boundary("bottom")

   {

    z=242;

   };
R_Date("IN68-9 241.5", 13100,200)

{

z=241.5;

};

R_Date("BIO I", 10450,90)

{

z=162.5;

};

R_Date("IN68-9", 9280,180)

{

z=156.5;

};

R_Date("BIO II", 9860,60)

{

z=155;

};
```

```
R_Date("BIO III", 9360,50)

{

z=143; };

R_Date("IN68-9  137.5", 9030,30)

{

z=137.5; };

R_Date("IN68-9 54.5", 6390,60)

{

z=54.5; };

R_Date("BIO IV", 5880,60)

{

z=43;

};

R_Date("IN68-9 10.5",3160,120)

{

z=11.5;

};


Boundary();
  };
  };
 };
```
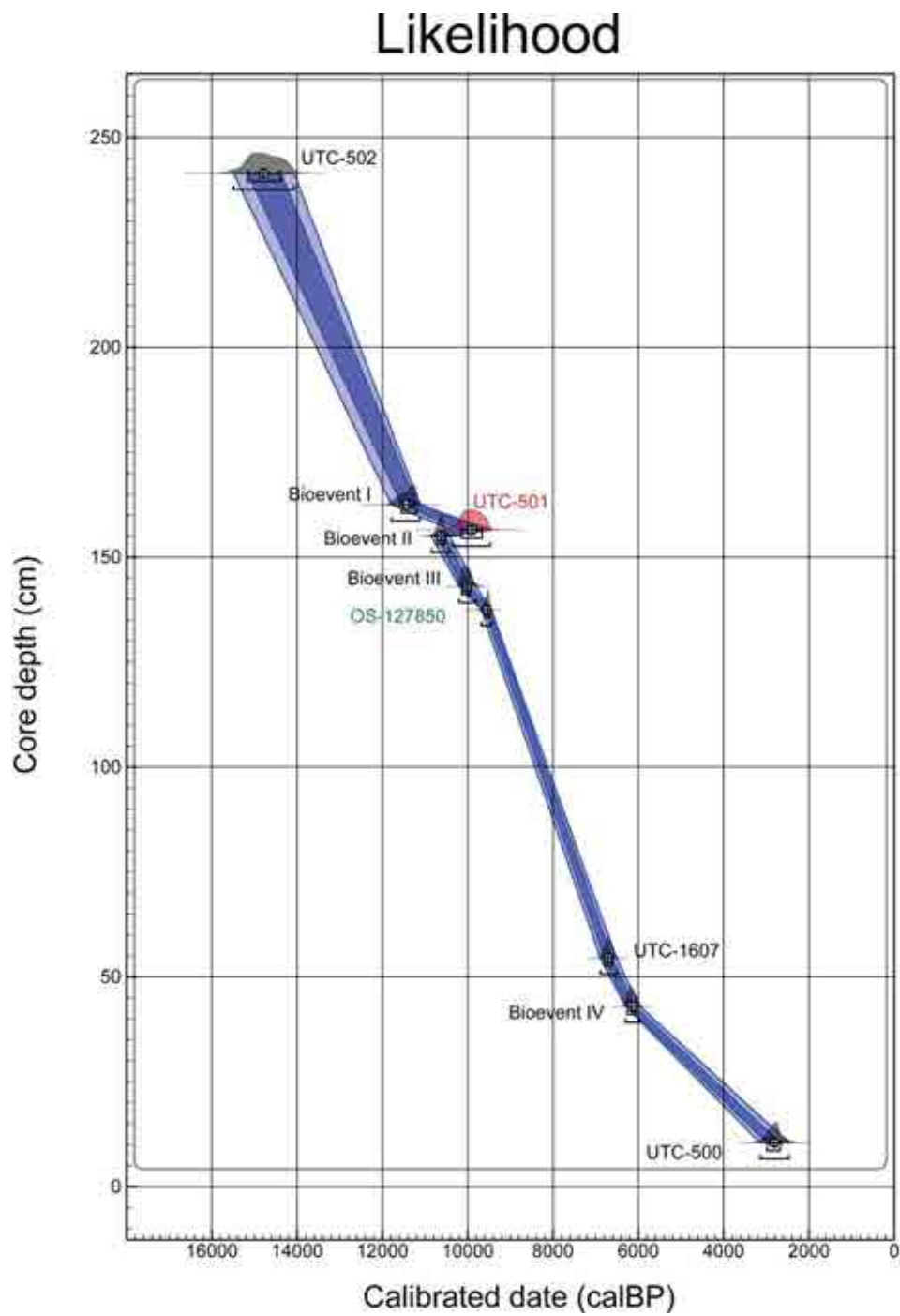
Fig. S1. Likelihood probability distributions of calibrated radiocarbon dates Light and dark blue show 1σ and 2σ, respectively.
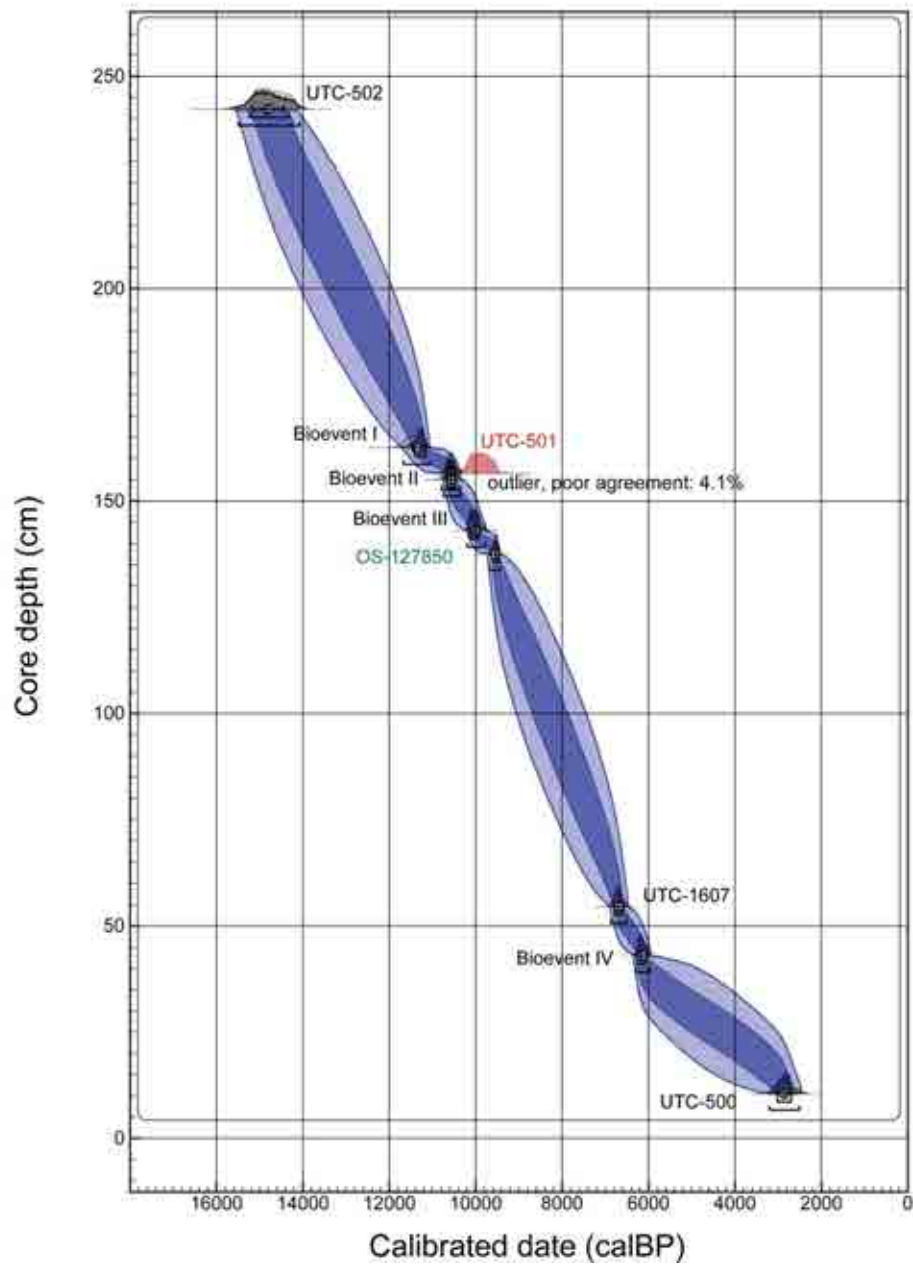
Fig. S2. Posterior probability distributions of calibrated radiocarbon dates Light and dark blue show 1σ and 2σ, respectively
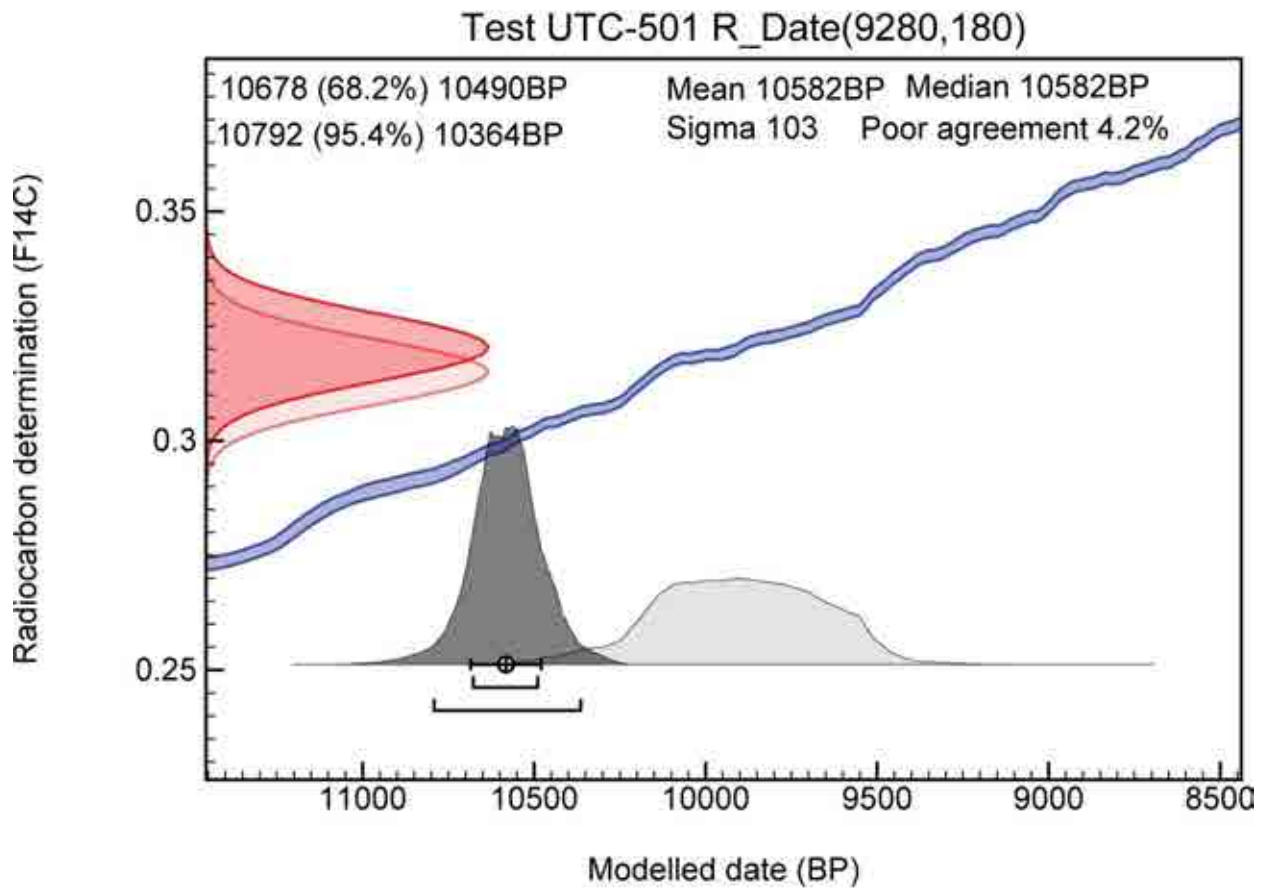
Fig. S3. Posterior probability distribution (dark grey) *vs* likelihood probability distribution (light gray) of test UTC-501.

Asioli, A., Trincardi, F., Lowe, J., Ariztegui, D., Langone, L., Oldfield, F., 2001. Sub-millennial scale climatic oscillations in the central Adriatic during the Lateglacial: palaeoceanographic implications. Quaternary Science Reviews 20, 1201-1221.

Favaretto, S., Asioli, A., Miola, A., Piva, A., 2008. Preboreal climatic oscillations recorded by pollen and foraminifera in the southern Adriatic Sea. Quaternary International 190, 89-102.

Rohling, E., Jorissen, F., De Stigter, H., 1997. 200 year interruption of Holocene sapropel formation in the Adriatic Sea. Journal of Micropalaeontology 16, 97-108.

Trincardi, F., Cattaneo, A., Asioli, A., Correggiari, A., Langone, L., 1996. Stratigraphy of the late-Quaternary deposits in the central Adriatic basin and the record of short-term climatic events. MEMORIE-ISTITUTO ITALIANO DI IDROBIOLOGIA 55, 39-70.

The Adriatic S1 is coeval with the Eastern Mediterranean S1 deposits

The Adriatic S1 onset is synchronous with the shutdown of the NAdDW

African monsoons weakened the LIW which in turn hampered the NAdDW formation